Macalester Journal of Physics and Astronomy

Volume 10
Issue 1 *Spring 2022*

Article 8

May 2022

The Survey of HI in Extremely Low-mass Dwarfs: New Results from VLA Imaging

Francesco Pecere
Macalester College, fpecere@macalester.edu

John M. Cannon
Macalester College, jcannon@macalester.edu

Damen Beverlin
Macalester College, dbeverli@macalester.edu

Jackson Codd
jcodd1@macalester.edu

The Survey of HI in Extremely Low-mass Dwarfs: New Results from VLA Imaging

Abstract

We present new HI spectral line imaging of 19 galaxies in the “Survey of HI in Extremely Low-mass Dwarfs” (SHIELD) acquired for Large Program VLA/ 20A-330. Using the National Radio Astronomy Observatory’s Karl G. Jansky Very Large Array (VLA) in the C configuration, we produce images of the neutral interstellar medium (HI) on angular scales of 15 to 20 arcseconds (corresponding to physical resolutions of 200 to 1100 parsecs). The three-dimensional cubes probe the morphology and kinematics of the gas at a range of spatial and spectral resolutions. The cubes were collapsed to produce two-dimensional moment maps (representing HI mass surface density and intensity weighted HI velocity). The HI gas was directly compared to the stellar component by comparison against optical and infrared imaging. In most cases, the gas and stars are co-spatial, with the exception of dwarfs with companion galaxies. The SHIELD galaxies are important to our understanding of galaxies’ properties at the low end of the mass spectrum.

Keywords

galaxies: evolution — galaxies: dwarf — galaxies: irregular

Draft version March 6, 2022
Typeset using LaTeX **twocolumn** style in AASTeX631

The Survey of HI in Extremely Low-mass Dwarfs: New Results from VLA Imaging

Francesco Pecere,[1] John M. Cannon,[1] Damon Beverlin,[1] and Jacskon Codd[1]

[1] *Department of Physics & Astronomy, Macalester College, 1600 Grand Avenue, Saint Paul, MN 55105, USA*

Abstract

We present new HI spectral line imaging of 19 galaxies in the "Survey of HI in Extremely Low-mass Dwarfs" (SHIELD) acquired for Large Program VLA/ 20A-330. Using the National Radio Astronomy Observatory's Karl G. Jansky Very Large Array (VLA) in the C configuration, we produce images of the neutral interstellar medium (HI) on angular scales of 15 to 20 arcseconds (corresponding to physical resolutions of 200 to 1100 parsecs). The three-dimensional cubes probe the morphology and kinematics of the gas at a range of spatial and spectral resolutions. The cubes were collapsed to produce two-dimensional moment maps (representing HI mass surface density and intensity weighted HI velocity). The HI gas was directly compared to the stellar component by comparison against optical and infrared imaging. In most cases, the gas and stars are co-spatial, with the exception of dwarfs with companion galaxies. The SHIELD galaxies are important to our understanding of galaxies' properties at the low end of the mass spectrum.

Keywords: galaxies: evolution — galaxies: dwarf — galaxies: irregular

1. INTRODUCTION

Galaxy is a word derived from the Greek "Galaxias" and it directly translates to "milky", named after our galaxy's appearance as a milky band of light in the sky. Galaxies are gravitationally bound systems of stars, gas, dust, and dark matter. They can be grouped into three different categories: spirals, galaxies with a central disc and spiral arms opening outwards; ellipticals, galaxies with an elliptical shape; irregulars, galaxies without a distinct shape. Irregulars, in turn, are divided into three major groups: irregulars with a vague structure (IrrI), irregulars without any distinct structure (IrrII), and dwarfs (dIrr) (Gallagher & Hunter 1984). Irregular dwarf galaxies are important to understanding galactic evolution because their composition, low metallicity, and abundance of HI gas, neutral hydrogen, resembles early galactic conditions. Galaxy formation is inversely related to stellar mass, meaning that smaller galaxies are more common than larger ones. This relation stops at low enough masses when the mass is not large enough to hold the galaxy together. The issue arises when trying to observe these smaller galaxies, this is because they are harder to observe due to their lower luminosity.

There have been various surveys that studied and analyzed dwarf irregular galaxies, such as FIGGS (Begum et al. 2008), Faint Irregular Galaxies GMRT Survey; LITTLE THINGS (Hunter et al. 2012), Local Irregulars That Trace Luminosity Extremes The HI Nearby Galaxy Survey; and VLA-ANGST (Ott et al. 2012), Very Large Array ACS Nearby Galaxy Survey Treasure. Although these surveys study dwarf irregulars, they focus on galaxies with a median HI mass of $10^{7.3}$, $10^{7.4}$, and $10^{7.9} M_{\odot}$ respectively (Cannon et al. 200)), while SHIELD, Survey of HI in Extremely Low-mass Dwarfs, focuses on galaxies with a median HI mass below $10^{7.2}$ $M_{\odot}$ (McQuinn et al. 2021). A galaxy's HI mass is measured via the intensity of the 21 cm line, caused by the spin-flip transition of neutral hydrogen's electron. This is a forbidden transition, occurring at a rate of $2.9 \cdot 10^{-15} s^{-1}$ (Wiese & Fuhr 2009). The ALFALFA, Arecibo Legacy Fast ALFA, project (Giovanelli et al. 2005) was designed, exploiting Arecibo's large collecting area and small beam size, to detect those galaxies in the local universe at the low end of the HI mass function. ALFALFA doesn't survey one specific part of the sky, but it fixes the telescope at one location and lets the sky drift over. In addition, it observes the same location twice at two different times, attempting to cancel out terrestrial interference. ALFALFA paved the way for research into low-mass dwarfs by detecting hundreds of galaxies with an HI mass below $10^{8} M_{\odot}$.

SHIELD is comprised of 82 galaxies which can help ascertain the low HI mass limit of the baryonic

Tully-Fisher relation and the Mass-Metallicity relation. here, we expand on 19 of the galaxies in the SHIELD group, bringing forth new observations of the HI matter from the VLA in the C configuration. These galaxies have all been cross-referenced with optical (McQuinn et al. 2021) and infrared (Klapkowski et al. 2020) catalogs.

2. DATA COLLECTION AND DATA REDUCTION

2.1. *VLA*

The 19 SHIELD galaxies (Table 1, columns 1-3) were observed twice using the Very Large Array (VLA) in New Mexico in the C configuration between March 22nd and June 1st, 2020 (Table 1, columns 4 and 5). The data was downloaded from the VLA and then analyzed in CASA. The dataset was trimmed keeping to keep the spectral window between 1536 MHz and 2559 MHz and flagged eliminating Radio Frequency interference (RFI). RFIs are caused by either man-made radio signals, Earth-based (electronic devices) and space-based (satellites), or naturally occurring (cosmic rays). They appear in four main ways: horizontal (across a specific time range), vertical (across a specific frequency range), point-like (across both an observing time and frequency range), or diffused (across a whole antenna). The dataset was then calibrated and reduced to produce a preliminary 3D cube. This was achieved using the commands "gaincal" to specify calibration values, "setjy" to fill the model column with the visibility of the calibrator, "bandpass" to calculate and calibrate the gain in frequency and time, "applycal" to apply calibration solutions to the dataset, "uvcontsub" to fit the continuum spectrum emissions and then subtract it from the channels selected, and "tclean" to reconstruct images from the visibilities.

After having produced a preliminary 3D cube for each observation, the two cubes were combined, cleaned to 2σ (Table 1, column 6), and then smoothed to 1.5 times the beam size (Table 1, column 7). The cube was then used to create two separate masks. The first was obtained by blanking to 2 times the baseline noise and the second by manually blanking. The two masks were then applied to the cube to produce a final 3D cube. The cube was then collapsed to produce $1e^{20}$, moment 0, and moment 1 maps (Figures 1-9). The $1e^{20}$ map shows the number of atoms, normalized to $1e^{20}$, for every cm^2. The moment 0 map shows the column density, i.e. the amount of HI gas. The moment 1 map shows the velocity gradient of the HI gas. The $1e^{20}$ map was then used to produce contours that were then overlaid on optical and infrared images of the galaxy (Figures 20-38). The final 3D cubes were also used to measure a galaxy's angle in the sky (Table 3, columns 2-3) and its rotational velocity (Table 3, columns 6-7). This was achieved by producing a position-velocity diagram for a slice drawn along the axis of rotation (Table 4, columns 2-6) (Figures 9-19).

2.2. *Legacy Survey*

The 19 SHIELD galaxies have been observed in the optical by the DESI Legacy Survey using the Blanco telescope at the Cerro Tololo Inter-American Observatory, the Mayall Telescope at the Kitt Peak National Observatory, and the University of Arizona Steward Observatory 2.3 m (90 inch) Bart Bok Telescope at Kitt Peak National Observatory. In this paper, the $1e^{20}$ map contours are overlaid on the Legacy Survey images for visual comparisons (Figures 20-38) of the locations of stellar material in these galaxies.

2.3. *Spitzer*

The 19 SHIELD galaxies have been observed in the infrared by the Spitzer telescope, analyzed, and then reduced (Klapkowski et al. 2020) to produce images at 3.6 µm. In this paper, the $1e^{20}$ map contours are overlaid on the Spitzer images for visual comparisons (Fig 20-38) of the locations of stellar material in these galaxies.

3. ANALYSIS AND DISCUSSION

3.1. *Scientific Methods*

A galaxy's HI mass (Table 2, columns 6-7) can be calculated from its distance from Earth (d) and its HI flux (S_{HI}) using equation 1,

$$M_{HI} = 2.356 \cdot 10^5 \cdot d^2 \cdot S_{HI} \qquad \text{(eq.1)}$$

where the $2.356 \cdot 10^5$ is a conversion factor that yields a result in solar masses from a distance in Mpc (Table 2, columns 2-3) and a flux in $Jy \cdot m/s$ (Table 2, columns 4-5). The error on the distances is reported only for those galaxies that have a distance estimate from the Hubble Space Telescope.

From the position-velocity slices (Figures 39-57), we can determine the apparent angle on the sky by looking at the extent of the offset. For simplicity, we chose to record half of this value ($\frac{\theta}{2}$) (Table 3, columns 2-3), in order to calculate the galactic radius (R) (Table 3, columns 4-5) instead of the diameter from the small angle equation, equation 2,

$$\frac{\theta}{2} = 206265 \cdot \frac{R}{d} \qquad \text{(eq.2)}$$

where d is the galaxy's distance from Earth (Table 2, columns 2-3) and 206265 is a conversion factor for the apparent angle on the sky in arcseconds. The error

on half of the apparent angle on the sky is recorded as half of the beam size.

In addition, from the position-velocity slices (Figures 39-57), we can determine the rotational velocity by recording half of the extent of the velocity range (V_r) (Table 3, columns 6-7). The total dynamic mass (M_dyn)(Table 3, columns 8-9) can then be derived from Newton's Universal Law of Gravitation and Centripetal Force, equation 3

$$M_{dyn} = \frac{V_r^2 \cdot R}{G} \quad \text{(eq.3)}$$

where R is the galactic radius and G is the universal gravitational constant ($G = 6.67 \cdot 10^{-11} \frac{m^3}{kg \cdot s^2}$). This value can be converted to solar masses by dividing by the mass of the sun ($M_\odot$). The error on the rotational velocity is recorded as 5 km/s because that is the sensitivity of the instrument, i.e. the velocity range of one pixel in the position-velocity slice.

The dynamic mass is the combination of the HI mass, stellar mass, and dark matter mass. In these low-mass dwarfs, the stellar mass is smaller than the HI mass and, for the sake of this analysis, can be neglected; therefore, the dark matter mass can be calculated by subtracting the HI mass to the Dynamic mass, equation 4

$$M_{dark-matter} = M_{dyn} - M_{HI} \quad \text{(eq.4)}$$

Josh Marine has been working on calculating the stellar mass of all 82 SHIELD galaxies. For 3 of these 19 SHIELD galaxies, the stellar mass has been determined (Table 2, column 8); therefore, the dark matter mass can be calculated by subtracting the HI and stellar mass to the Dynamic mass (Table 3, columns 10-11), equation 5

$$M_{dark-matter} = M_{dyn} - M_{HI} - M_{stellar} \quad \text{(eq.5)}$$

3.2. *Galaxies*

AGC 221089: This galaxy is moving away at an average velocity of 1090 km/s, is 9.10 Mpc away from Earth, and has an HI flux of 0.72 ± 0.05 $\frac{Jy \cdot km}{s}$. From this, we determine that HI mass is $1.40 \cdot 10^7 \pm 9.76 \cdot 10^5$ $M_\odot$. AGC 221089 has a galactic radius of 882 ± 331 pc, a velocity range between 1120 km/s and 1070 km/s, and a rotational velocity of $2.50 \cdot 10^4 \pm 5.00 \cdot 10^3$ m/s. From this, the Dynamical mass is determined to be $1.28 \cdot 10^8 \pm 7.03 \cdot 10^7$ $M_\odot$. Therefore, the estimated Dark Matter mass is $1.14 \cdot 10^8 \pm 7.03 \cdot 10^7$ $M_\odot$ or 89.05 % of the total mass. From the Legacy Survey and Spitzer images, we see that the bulk of the stellar population is located in the same position as the highest density of HI.

AGC 223231:This galaxy is moving away at an average velocity of 695 km/s, iis 8.32 ± 0.21 Mpc away from Earth, and has an HI flux of 0.97 ± 0.04 $\frac{Jy \cdot km}{s}$. From this, we determine that HI mass is $1.58 \cdot 10^7 \pm 1.03 \cdot 10^6$ $M_\odot$. In addition, the stellar mass has been measured to be $5.62 \cdot 10^6$ $M_\odot$. AGC 223231 has a galactic radius of 2017 ± 307 pc, a velocity range between 610 km/s and 580 km/s, and a rotational velocity of $1.75 \cdot 10^4 \pm 5.00 \cdot 10^3$ m/s. From this, the Dynamical mass is determined to be $1.44 \cdot 10^8 \pm 8.50 \cdot 10^7$ $M_\odot$. Therefore, the estimated Dark Matter mass is $1.22 \cdot 10^8 \pm 8.50 \cdot 10^7$ $M_\odot$ or 85.07 % of the total mass. From the Legacy Survey and Spitzer images, we see that the bulk of the stellar population is located in the same position as the highest density of HI.

AGC 223254: This galaxy is moving away at an average velocity of 625 km/s, is 6.41 ± 0.09 Mpc away from Earth, and has an HI flux of 1.16 ± 0.04 $\frac{Jy \cdot km}{s}$. From this, we determine that HI mass is $1.12 \cdot 10^7 \pm 4.99 \cdot 10^5$ $M_\odot$. AGC 223254 has a galactic radius of 1243 ± 234 pc, a velocity range between 640 km/s and 610 km/s, and a rotational velocity of $1.50 \cdot 10^4 \pm 5.00 \cdot 10^3$ m/s. From this, the Dynamical mass is determined to be $6.51 \cdot 10^7 \pm 4.51 \cdot 10^7$ $M_\odot$. Therefore, the estimated Dark Matter mass is $5.38 \cdot 10^8 \pm 4.51 \cdot 10^7$ $M_\odot$ or 82.74 % of the total mass. From the Legacy Survey and Spitzer images, we see that the bulk of the stellar population is not located in the same position as the highest density of HI. If we expand the field of view, we observe that AGC 223254 is interacting with UGC 7603. The two galaxies are separated by 1980 arcseconds in the sky, AGC 223254 is 6.41 Mpc away from Earth, while UGC 7603 is 6.61 Mpc. This means that their physical separation is around 60-65 kpc, or about 60 % of the diameter of the Milky Way. The gas in AGC 223254 is attracted towards UGC 7603 due to its dissipational nature, while the stars are not.

AGC 229052: This galaxy is moving away at an average velocity of 820 km/s, is 9.5 Mpc away from Earth, and has an HI flux of 0.51 ± 0.04 $\frac{Jy \cdot km}{s}$. From this, we determine that HI mass is $1.08 \cdot 10^7 \pm 8.51 \cdot 10^5$ $M_\odot$. AGC 229052 has a galactic radius of 921 ± 345 pc, a velocity range between 225 km/s and 795 km/s, and a rotational velocity of $1.50 \cdot 10^4 \pm 5.00 \cdot 10^3$ m/s. From this, the Dynamical mass is determined to be $4.82 \cdot 10^7 \pm 3.69 \cdot 10^7$ $M_\odot$. Therefore, the estimated Dark Matter mass is $3.74 \cdot 10^7 \pm 3.69 \cdot 10^7$ $M_\odot$ or 77.50 % of the total mass. From the Legacy Survey and Spitzer images, we see that the bulk of the stellar population is located in the same position as the highest density of HI.

AGC 229053: This galaxy is moving away at an average

velocity of 435 km/s, is 12.5 ± 0.26 Mpc away from Earth, and has an HI flux of 0.77 ± 0.04 $\frac{Jy \cdot km}{s}$. From this, we determine that HI mass is $2.83 \cdot 10^7 \pm 1.89 \cdot 10^6$ $M_\odot$. In addition, the stellar mass has been measured to be $8.91 \cdot 10^6$ $M_\odot$. AGC 229053has a galactic radius of 2424 ± 457 pc, a velocity range between 460 km/s and 410 km/s, and a rotational velocity of $2.50 \cdot 10^4$ ± $5.00 \cdot 10^3$ m/s. From this, the Dynamical mass is determined to be $3.52 \cdot 10^8 \pm 1.56 \cdot 10^8$ $M_\odot$. Therefore, the estimated Dark Matter mass is $3.15 \cdot 10^8 \pm 1.56 \cdot 10^8$ $M_\odot$ or 89.43 % of the total mass. From the Legacy Survey and Spitzer images, we see that the bulk of the stellar population is located in the same position as the highest density of HI.

AGC 229090: This galaxy is moving away at an average velocity of 550 km/s, is 7.1 Mpc away from Earth, and has an HI flux of 1.13 ± 0.06 $\frac{Jy \cdot km}{s}$. From this, we determine that HI mass is $1.34 \cdot 10^7 \pm 7.13 \cdot 10^5$ $M_\odot$. AGC 229090 has a galactic radius of 1033 ± 258 pc, a velocity range between 570 km/s and 520 km/s, and a rotational velocity of $2.50 \cdot 10^4 \pm 5.00 \cdot 10^3$ m/s. From this, the Dynamical mass is determined to be $1.50 \cdot 10^8$ ± $7.08 \cdot 10^7$ $M_\odot$. Therefore, the estimated Dark Matter mass is $1.37 \cdot 10^8 \pm 7.08 \cdot 10^7$ $M_\odot$ or 91.06 % of the total mass. From the Legacy Survey and Spitzer images, we see that the bulk of the stellar population is located in the same position as the highest density of HI.

AGC 229284: This galaxy is moving away at an average velocity of 1230 km/s, is 9.4 Mpc away from Earth, and has an HI flux of 0.54 ± 0.04 $\frac{Jy \cdot km}{s}$. From this, we determine that HI mass is $1.27 \cdot 10^7 \pm 8.33 \cdot 10^5$ $M_\odot$. AGC 229284 has a galactic radius of 1139 ± 342 pc, a velocity range between 1245 km/s and 1210 km/s, and a rotational velocity of $1.75 \cdot 10^4 \pm 5.00 \cdot 10^3$ m/s. From this, the Dynamical mass is determined to be $8.12 \cdot 10^7$ ± $5.24 \cdot 10^7$ $M_\odot$. Therefore, the estimated Dark Matter mass is $6.00 \cdot 10^7 \pm 5.24 \cdot 10^7$ $M_\odot$ or 86.15 % of the total mass. From the Legacy Survey and Spitzer images, we see that the bulk of the stellar population is located in the same position as the highest density of HI.

AGC 229379: This galaxy is moving away at an average velocity of 645 km/s, is 7.51 ± 0.29 Mpc away from Earth, and has an HI flux of 0.38 ± 0.04 $\frac{Jy \cdot km}{s}$. From this, we determine that HI mass is $5.05 \cdot 10^6 \pm 6.59 \cdot 10^5$ $M_\odot$. AGC 229379 has a galactic radius of 728 ± 275 pc, a velocity range between 660 km/s and 630 km/s, and a rotational velocity of $1.50 \cdot 10^4 \pm 5.00 \cdot 10^3$ m/s. From this, the Dynamical mass is determined to be $3.18 \cdot 10^7$ ± $2.92 \cdot 10^7$ $M_\odot$. Therefore, the estimated Dark Matter mass is $3.31 \cdot 10^7 \pm 2.92 \cdot 10^7$ $M_\odot$ or 86.75 % of the total mass. From the Legacy Survey and Spitzer images, we see that the bulk of the stellar population is located in the same position as the highest density of HI.

AGC 229439: This galaxy is moving away at an average velocity of 865 km/s, is 11.9 Mpc away from Earth and, has an HI flux of 0.41 ± 0.04 $\frac{Jy \cdot km}{s}$. From this, we determine that HI mass is $1.37 \cdot 10^7 \pm 1.33 \cdot 10^6$ $M_\odot$. AGC 229439 has a galactic radius of 2308 ± 433 pc, a velocity range between 885 km/s and 845 km/s, and a rotational velocity of $2.00 \cdot 10^4 \pm 5.00 \cdot 10^3$ m/s. From this, the Dynamical mass is determined to be $2.15 \cdot 10^8$ ± $1.15 \cdot 10^8$ $M_\odot$. Therefore, the estimated Dark Matter mass is $2.01 \cdot 10^8 \pm 1.15 \cdot 10^8$ $M_\odot$ or 93.63 % of the total mass. From the Legacy Survey and Spitzer images, we see that the bulk of the stellar population is located slightly off-center from the position of the highest density of HI.

AGC 238890: This galaxy is moving away at an average velocity of 365 km/s, is 5.34 ± 0.07 Mpc away from Earth, and has an HI flux of 0.35 ± 0.04 $\frac{Jy \cdot km}{s}$. From this, we determine that HI mass is $2.35 \cdot 10^6 \pm 2.76 \cdot 10^5$ $M_\odot$. AGC 238890 has a galactic radius of 518 ± 194 pc, a velocity range between 380 km/s and 350 km/s, and a rotational velocity of $1.50 \cdot 10^4 \pm 5.00 \cdot 10^3$ m/s. From this, the Dynamical mass is determined to be $2.71 \cdot 10^7$ ± $2.07 \cdot 10^7$ $M_\odot$. Therefore, the estimated Dark Matter mass is $2.47 \cdot 10^7 \pm 2.07 \cdot 10^7$ $M_\odot$ or 91.32 % of the total mass. From the Legacy Survey and Spitzer images, we see that the bulk of the stellar population is located slightly off-center from the position of the highest density of HI.

AGC 239031: This galaxy is moving away at an average velocity of 845 km/s, is 10.9 Mpc away from Earth, and has an HI flux of 0.46 ± 0.04 $\frac{Jy \cdot km}{s}$. From this, we determine that HI mass is $1.29 \cdot 10^7 \pm 1.12 \cdot 10^6$ $M_\odot$. AGC 239031 has a galactic radius of 1057 ± 194 pc, a velocity range between 860 km/s and 820 km/s, and a rotational velocity of $2.00 \cdot 10^4 \pm 5.00 \cdot 10^3$ m/s. From this, the Dynamical mass is determined to be $9.83 \cdot 10^7$ ± $6.15 \cdot 10^7$ $M_\odot$. Therefore, the estimated Dark Matter mass is $8.55 \cdot 10^7 \pm 6.15 \cdot 10^7$ $M_\odot$ or 86.91 % of the total mass. From the Legacy Survey and Spitzer images, we see that the bulk of the stellar population is located slightly off-center from the position of the highest density of HI.

AGC 322463: This galaxy is moving away at an average velocity of 350 km/s, is 6.5 Mpc away from Earth, and has an HI flux of 0.90 ± 0.05 $\frac{Jy \cdot km}{s}$. From this, we determine that HI mass is $8.96 \cdot 10^6 \pm 4.98 \cdot 10^5$ $M_\odot$. AGC 322463 has a galactic radius of 630 ± 236 pc, a velocity range between 365 km/s and 325 km/s, and a rotational velocity of $2.00 \cdot 10^4 \pm 5.00 \cdot 10^3$ m/s. From this, the Dynamical mass is determined to be $5.86 \cdot 10^7$ ± $3.66 \cdot 10^7$ $M_\odot$. Therefore, the estimated Dark Matter

mass is $4.97 \cdot 10^7 \pm 3.67 \cdot 10^7$ $M_\odot$ or 84.72 % of the total mass. From the Legacy Survey and Spitzer images, we see that the bulk of the stellar population is located slightly off-center from the position of the highest density of HI.

AGC 724906: This galaxy is moving away at an average velocity of 950 km/s, is 9.1 Mpc away from Earth, and has an HI flux of 0.78 ± 0.03 $\frac{Jy \cdot km}{s}$. From this, we determine that HI mass is $1.52 \cdot 10^7 \pm 5.85 \cdot 10^5$ $M_\odot$. AGC 724906 has a galactic radius of 1765 ± 331 pc, a velocity range between 965 km/s and 930 km/s, and a rotational velocity of $1.75 \cdot 10^4 \pm 5.00 \cdot 10^3$ m/s. From this, the Dynamical mass is determined to be $1.26 \cdot 10^8 \pm 7.56 \cdot 10^7$ $M_\odot$. Therefore, the estimated Dark Matter mass is $1.10 \cdot 10^8 \pm 7.56 \cdot 10^7$ $M_\odot$ or 87.89 % of the total mass. From the Legacy Survey and Spitzer images, we see that the bulk of the stellar population is located slightly off-center from the position of the highest density of HI.

AGC 728909: This galaxy is moving away at an average velocity of 725 km/s, is 10.2 Mpc away from Earth, and has an HI flux of 0.55± 0.05 $\frac{Jy \cdot km}{s}$. From this, we determine that HI mass is $1.35 \cdot 10^7 \pm 1.23 \cdot 10^6$ $M_\odot$. AGC 728909 has a galactic radius of 989 ± 371 pc, a velocity range between 740 km/s and 705 km/s, and a rotational velocity of $1.75 \cdot 10^4 \pm 5.00 \cdot 10^3$ m/s. From this, the Dynamical mass is determined to be $7.04 \cdot 10^7 \pm 4.82 \cdot 10^7$ $M_\odot$. Therefore, the estimated Dark Matter mass is $5.70 \cdot 10^7 \pm 4.82 \cdot 10^7$ $M_\odot$ or 80.86 % of the total mass. From the Legacy Survey and Spitzer images, we see that the bulk of the stellar population is located slightly off-center from the position of the highest density of HI.

AGC 732041: This galaxy is moving away at an average velocity of 1190 km/s, is 9.2 Mpc away from Earth, and has an HI flux of 0.30± 0.03 $\frac{Jy \cdot km}{s}$. From this, we determine that HI mass is $5.98 \cdot 10^6 \pm 5.98 \cdot 10^5$ $M_\odot$. AGC 723041 has a galactic radius of 1115 ± 335 pc, a velocity range between 1210 km/s and 1170 km/s, and a rotational velocity of $2.00 \cdot 10^4 \pm 5.00 \cdot 10^3$ m/s. From this, the Dynamical mass is determined to be $1.04 \cdot 10^8 \pm 6.05 \cdot 10^7$ $M_\odot$. Therefore, the estimated Dark Matter mass is $9.78 \cdot 10^7 \pm 6.05 \cdot 10^7$ $M_\odot$ or 94.23 % of the total mass. From the Legacy Survey and Spitzer images, we see that the bulk of the stellar population is located slightly off-center from the position of the highest density of HI.

AGC 732129: This galaxy is moving away at an average velocity of 1070 km/s, is 9.3 Mpc away from Earth, and has an HI flux of 0.53 ± 0.03 $\frac{Jy \cdot km}{s}$. From this, we determine that HI mass is $1.08 \cdot 10^7 \pm 6.11 \cdot 10^5$ $M_\odot$. AGC 732129 has a galactic radius of 902 ± 338 pc, a velocity range between 1090 km/s and 1050 km/s, and a rotational velocity of $2.00 \cdot 10^4 \pm 5.00 \cdot 10^3$ m/s. From this, the Dynamical mass is determined to be $8.39 \cdot 10^7 \pm 5.24 \cdot 10^7$ $M_\odot$. Therefore, the estimated Dark Matter mass is $7.31 \cdot 10^7 \pm 5.24 \cdot 10^7$ $M_\odot$ or 87.13 % of the total mass. From the Legacy Survey and Spitzer images, we see that the bulk of the stellar population is located slightly off-center from the position of the highest density of HI.

AGC 732226: This galaxy is moving away at an average velocity of 1335 km/s, is 9.0 Mpc away from Earth, and has an HI flux of 0.64 ± 0.05 $\frac{Jy \cdot km}{s}$. From this, we determine that HI mass is $1.22 \cdot 10^7 \pm 9.54 \cdot 10^5$ $M_\odot$. AGC 732226 has a galactic radius of 1309 ± 327 pc, a velocity range between 1350 km/s and 1320 km/s, and a rotational velocity of $1.50 \cdot 10^4 \pm 5.00 \cdot 10^3$ m/s. From this, the Dynamical mass is determined to be $6.85 \cdot 10^7 \pm 4.88 \cdot 10^7$ $M_\odot$. Therefore, the estimated Dark Matter mass is $5.63 \cdot 10^7 \pm 4.88 \cdot 10^7$ $M_\odot$ or 82.17 % of the total mass. From the Legacy Survey and Spitzer images, we see that the bulk of the stellar population is located slightly off-center from the position of the highest density of HI.

AGC 732418: This galaxy is moving away at an average velocity of 1025 km/s, is 9.3 Mpc away from Earth, and has an HI flux of 0.27 ± 0.04 $\frac{Jy \cdot km}{s}$. From this, we determine that HI mass is $5.50 \cdot 10^6 \pm 8.15 \cdot 10^5$ $M_\odot$. AGC 732418 has a galactic radius of 902 ± 338 pc, a velocity range between 1040 km/s and 1015 km/s, and a rotational velocity of $1.25 \cdot 10^4 \pm 5.00 \cdot 10^3$ m/s. From this, the Dynamical mass is determined to be $3.28 \cdot 10^7 \pm 2.90 \cdot 10^7$ $M_\odot$. Therefore, the estimated Dark Matter mass is $2.73 \cdot 10^7 \pm 2.90 \cdot 10^7$ $M_\odot$ or 83.21 % of the total mass. From the Legacy Survey and Spitzer images, we see that the bulk of the stellar population is located slightly off-center from the position of the highest density of HI.

AGC 742601: This galaxy is moving away at an average velocity of 565 km/s, is 7.00 ± 0.18 Mpc away from Earth, and has an HI flux of 0.88 ± 0.06 $\frac{Jy \cdot km}{s}$. From this, we determine that HI mass is $1.02 \cdot 10^7 \pm 8.68 \cdot 10^5$ $M_\odot$. In addition, the stellar mass has been measured to be $4.37 \cdot 10^6$ $M_\odot$. AGC 742601has a galactic radius of 1018 ± 256 pc, a velocity range between 575 km/s and 535 km/s, and a rotational velocity of $2.50 \cdot 10^4 \pm 5.00 \cdot 10^3$ m/s. From this, the Dynamical mass is determined to be $1.48 \cdot 10^8 \pm 6.99 \cdot 10^7$ $M_\odot$. Therefore, the estimated Dark Matter mass is $1.33 \cdot 10^8 \pm 6.99 \cdot 10^7$ $M_\odot$ or 90.19 % of the total mass. From the Legacy Survey and Spitzer images, we see that the bulk of the stellar population is located in the same position as the

highest density of HI.

4. SUMMARY

SHIELD is a systematic investigation of low-mass dwarf galaxies to study and characterize their major properties as a function of HI mass. This paper has presented new observations of 19 of the 82 SHIELD galaxies, producing $1 \cdot e^{20}$, moment 0, and moment 1 maps, alongside $1 \cdot e^{20}$ contour overlays of optical and infrared images and Position-Velocity slices. From these results, we were able to put forward estimates of these galaxies' HI masses, galactic radii, rotational velocities, and Dark Matter masses. The galaxies have HI masses between $2.35 \cdot 10^6$ $M_\odot$ and $2.83 \cdot 10^7$ $M_\odot$ or $log_{10} M_H I = 10^{6.37}$ and $log_{10} M_H I = 10^{7.45}$, with an average HI mass of $1.16 \pm 0.55 \cdot 10^6$ $M_\odot$ or $log_{10} M_H I = 10^{7.07 \pm 0.23}$. The Dark Matter component of these galaxies is between $2.47 \cdot 10^7$ $M_\odot$ and $3.15 \cdot 10^8$ $M_\odot$ or $log_{10} M_D M = 10^{7.39}$ and $log_{10} M_D M = 10^{8.50}$, with an average Dark Matter mass of $9.47 \pm 7.03 \cdot 10^7$ $M_\odot$ or $log_{10} M_D M = 10^{7.88 \pm 0.29}$. Lastly, the Dark Matter component makes up between 77.50% and 94.23%, with an average make up of 86.84 $\pm$ 4.38 %. In the future, this work can be expanded on by analyzing all 82 SHIELD galaxies or observing the 19 SHIELD galaxies, described in this paper, in other VLA configurations. The first would allow us to get a more holistic image of these galaxies and their properties; while the second will allows us to produce more detailed images of the galaxies. In addition, the galaxies, could be placed on the Baryonic Tully-Fisher relation, allowing us to study their dark matter and rotational velocity properties.

5. ACKNOWLEDGEMENTS

John M. Cannon is supported by NSF grant AST2009894. The authors are grateful to Macalester College and to the University of Minnesota REU Program for supporting this project.

Facility: VLA

REFERENCES

[Begum et al. 2008]Begum, A., Chengalur, J. N., Karachenstev, I. D. et al. 2008, MNRAS, 386, 1667. doi:10.1111/j.1365-2966.2008.13150.x

[Cannon et al. 200)]Cannon, J. M., Giovanelli, R., Haynes, M. P. et al. 2011, ApJL, 739. L22. doi:10.1088/2041-8205/739/1/L22

[Gallagher & Hunter 1984]Gallagher, J. S. III & Hunter, D. A 1984, ARA&, 22,37

[Giovanelli et al. 2005]Giovanelli, R., Haynes, M. P., Kent, B. R., et al. 2005, AJ, 130, 2598. doi:10.1086/497431

[Hunter et al. 2012]Hunter, D. A., Ficut-Vicas, D., Ashley, T., et al. 2012, AJ, 144, 134. doi: 10.1088/0004-6256/144/5/134

[Klapkowski et al. 2020]Klapkowski, M., Cannon, J. M., Adams, E., et al. 2020, BAAS, 235, 168.

[McQuinn et al. 2021]McQuinn, K. B. W., Telidevara, A. K., Fuson, J., et al. 2021, ApJ, 918, 23. doi:10.3847/1538-4357/ac03ae

[Ott et al. 2012]Ott, J., Stilp, A. M., Warren, S, R. et al. 2012, AJ, 144, 123. doi:10.1088/0004-6256/144/4/123

[Wiese & Fuhr 2009]Wiese, W. L. & Fuhr, J. R. 2009, JPCRD, 38, 565. doi:10.1063/1.3077727

Table 1. Details of the observations of the 19 SHIELD galaxies

Galaxy	RA	Dec	First Observation Date	Second Observation Date	RMS	Beam Size
AGC	(J2000)	(J2000)	and Time (UTC)	and Time (UTC)	Jy	("x")
221089	12:53:10:0	+25:16:41	May 25, 00:20:21.0 - May 25, 02:49:51.0	May 25, 22:45:57.0 - May 25, 01:15:30.0	0.00066	19.73 x 15.99
223231	12:22:52.7	+33:49:43	May 21, 23:59:48.0 - May 22, 02:29:18.0	May 23, 22:43:03.0 - May 24, 01:12:33.0	0.00079	18.46 x 16.52
223254	12:28:05:0	+22:17:27	Jun 01, 02:30:24.0 - Jun 01, 04:59:51.0	May 12, 05:39:12.0 - May 24, 08:08:45.0	0.00056	18.30 x 16.85
229052	12:20:41.1	+24:57:21	May 15, 00:20:42.0 - May 15, 02:50:15.0	May 16, 05:45:48.0 - May 16, 08:15:21.0	0.00063	18.87 x 16.46
229053	12:18:15.5	+25:34:05	Apr 18, 06:21:36.0 - Apr 18, 08:51:06.0	Apr 20, 01:49:15.0 - Apr 20, 04:18:45.0	0.00056	18.65 x 17.32
229090	12:36:49.7	+33:36:48	May 04, 06:20:09.0 - May 04, 08:49:42.0	May 06, 01:49:15.0 - May 06, 04:18:45.1	0.00060	18.43 x 16.78
229284	12:17:14.6	+28:36:14	May 15, 04:50:03.0 - May 15, 07:19:30.0	May 17, 00:19:54.0 - May 17, 02:49:24.0	0.00055	18.76 x 17.05
229379	12:30:34.3	+23:12:19	May 12, 23:41:39.0 - May13, 02:10:15.0	May 13, 02:10:24.0 - May 13, 04:39:51:0	0.00063	18.48 x 16.35
229439	12:51:39.5	+32:10:50	May 05, 05:21:30.0 - May 05, 07:51:00.0	May 18, 00:28:09.0 - May 18, 02:57:36.0	0.00058	18.07 x 16.51
238890	13:32:30.3	+25:07:24	Apr 27, 03:28:12.0 - Apr 27, 05:57:53.0	May 11, 06:47:27.0 - May 11, 09:16:57.0	0.00057	18.21 x 17.78
239031	13:08:12.4	+29:05:15	May 04, 03:50:33.0 - May 04, 06:20:03.0	May 05, 02:51:54.0 - May 05, 05:21:21.0	0.00059	17.49 x 15.14
322463	22:59:35.6	+16:45:56	Mar 22, 19:18:03.0 - Mar 22, 21:47:36.0	Mar 24, 19:59:18.0 - Mar 24, 22:28:48.0	0.00059	21.42 x 16.74
724906	12:30:56.0	+26:30:41	May 19, 04:31:18.0 - May 19, 07:00:48.0	May 20, 03:24:45.0 - May 20, 05:54:15.0	0.00069	16.59 x 15.92
728909	13:22:27.6	+35:12:19	May 13, 07:09:36.0 - May 13, 09:39:06.0	My 30, 04:42:54.0 - May 30, 07:12:24.0	0.00062	18.60 x 16.42
732041	12:17:42.4	+27:29:03	Apr 29, 01:25:39.0 - Apr 18, 03:55:09.0	Apr 30, 00:40:03.0 - Apr 30, 03:09:33.0	0.00059	17.96 x 16.51
732129	12:27:25.2	+27:50:27	May 11, 23:45:03.0 - May 22, 02:14:33.0	May 12, 02:14:39.0 - May 12, 04:44:12.00	0.00056	18.77 x 17.14
732226	12:40:48.5	+25:56:40	May 26, 01:15:36.0 - May 26, 03:45:06.0	May 28, 01:16:51.0 - May 28, 03:46:21.0	0.00060	16.67 x 15.01
732418	12:59:08.2	+26:22:39	May 07, 07:11:12.0 - May 07, 09:40:42.0	May 20, 05:54:21.0 - May 20, 08:23:54.0	0.00058	20.04 x 17.00
742601	12:49:36.9	+21:55:05	May 17, 04:59:03.0 - May 17, 07:28:36.0	May 28, 03:46:27.0 - May 28, 06:16:00.0	0.00062	17.14 x 16.31

Table 2. HI and Stellar Mass

Galaxy AGC	Distance (Mpc)	err (Mpc)	HI flux (Jy km/s)	err (Jy km/s)	HI mass ($M_\odot$)	err ($M_\odot$)	Stellar Mass ($M_\odot$)
221089	9.10	0.00	0.72	0.05	1.40E+07	9.76E+05	
223231	8.32	0.21	0.97	0.04	1.58E+07	1.03E+06	5.62E+06
223254	6.41	0.09	1.16	0.04	1.12E+07	4.99E+05	
229052	9.50	0.00	0.51	0.04	1.08E+07	8.51E+05	
229053	12.50	0.26	0.77	0.04	2.83E+07	1.89E+06	8.91E+06
229090	7.10	0.00	1.13	0.06	1.34E+07	7.13E+05	
229284	9.40	0.00	0.54	0.04	1.12E+07	8.33E+05	
229379	7.51	0.29	0.38	0.04	5.05E+06	6.59E+05	
229439	11.90	0.00	0.41	0.04	1.37E+07	1.33E+06	
238890	5.34	0.07	0.35	0.04	2.35E+06	2.76E+05	
239031	10.90	0.00	0.46	0.04	1.29E+07	1.12E+06	
322463	6.50	0.00	0.9	0.05	8.96E+06	4.98E+05	
724906	9.10	0.00	0.78	0.03	1.52E+07	5.85E+05	
728909	10.20	0.00	0.55	0.05	1.35E+07	1.23E+06	
732041	9.20	0.00	0.3	0.03	5.98E+06	5.98E+05	
732129	9.30	0.00	0.53	0.03	1.08E+07	6.11E+05	
732226	9.00	0.00	0.64	0.05	1.22E+07	9.54E+05	
732418	9.30	0.00	0.27	0.04	5.50E+06	8.15E+05	
742601	7.00	0.18	0.88	0.06	1.02E+07	8.68E+05	4.37E+06

Table 3. Dark Matter Analysis

Galaxy	$\theta/2$	err	Radius	err	Rotational Velocity	err	Dynamic Mass	err	Dark Matter	err	% Dark Matter
AGC	(")	(")	(pc)	(pc)	(m/s)	(m/s)	($M_\odot$)	($M_\odot$)	($M_\odot$)	($M_\odot$)	(%)
221089	20.0	7.5	882	331	2.50E+04	5.00E+03	1.28E+08	7.03E+07	1.14E+08	7.03E+07	89.05
223231	50.0	7.5	2017	307	1.75E+04	5.00E+03	1.44E+08	8.50E+07	1.22E+08	8.50E+07	85.07
223254	40.0	7.5	1243	234	1.50E+04	5.00E+03	6.51E+07	4.51E+07	5.38E+07	4.51E+07	82.74
229052	20.0	7.5	921	345	1.50E+04	5.00E+03	4.82E+07	3.69E+07	3.74E+07	3.69E+07	77.50
229053	40.0	7.5	2424	457	2.50E+04	5.00E+03	3.52E+08	1.56E+08	3.15E+08	1.56E+08	89.43
229090	30.0	7.5	1033	258	2.50E+04	5.00E+03	1.50E+08	7.08E+07	1.37E+08	7.08E+07	91.06
229284	25.0	7.5	1139	342	1.75E+04	5.00E+03	8.12E+07	5.24E+07	6.99E+07	5.24E+07	86.15
229379	20.0	7.5	728	275	1.50E+04	5.00E+03	3.81E+07	2.92E+07	3.31E+07	2.92E+07	86.75
229439	40.0	7.5	2308	433	2.00E+04	5.00E+03	2.15E+08	1.15E+08	2.01E+08	1.15E+08	93.63
238890	20.0	7.5	518	194	1.50E+04	5.00E+03	2.71E+07	2.07E+07	2.47E+07	2.07E+07	91.32
239031	20.0	7.5	1057	396	2.00E+04	5.00E+03	9.83E+07	6.15E+07	8.55E+07	6.15E+07	86.91
322463	20.0	7.5	630	236	2.00E+04	5.00E+03	5.86E+07	3.66E+07	4.97E+07	3.67E+07	84.72
724906	40.0	7.5	1765	331	1.75E+04	5.00E+03	1.26E+08	7.56E+07	1.10E+08	7.56E+07	87.89
728909	20.0	7.5	989	371	1.75E+04	5.00E+03	7.04E+07	4.82E+07	5.70E+07	4.82E+07	80.86
732041	25.0	7.5	1115	335	2.00E+04	5.00E+03	1.04E+08	6.05E+07	9.78E+07	6.05E+07	94.23
732129	20.0	7.5	902	338	2.00E+04	5.00E+03	8.39E+07	5.24E+07	7.31E+07	5.24E+07	87.13
732226	30.0	7.5	1309	327	1.50E+04	5.00E+03	6.85E+07	4.88E+07	5.63E+07	4.88E+07	82.17
732418	20.0	7.5	902	338	1.25E+04	5.00E+03	3.28E+07	2.90E+07	2.73E+07	2.90E+07	83.21
742601	30.0	7.5	1018	256	2.50E+04	5.00E+03	1.48E+08	6.99E+07	1.33E+08	6.99E+07	90.19

Table 4. Position-Velocity Slicing

Galaxy AGC	Start Point (RA x dec)	End Point (RA x dec)	Position Angle (degrees)	Length (arcminutes)	Averaging Width
221089	12:53:19.2 x +25:14:50	12:53:00.6 x +25:18:55	134.16	5.848	5
223231	12:22:55.0 x +33:48:46	12:22:48.8 x +33:50:38	144.92	2.272	5
223254	12:28:01.8 x + 22:16:26	12:28:09.2 x +22:18:11	44.01	2.448	5
229052	12:20:37.5 x +24:56:34	12:20:43.8 x +24:58:07	42.78	2.126	5
229053	12:18:11.6 x +25:32:33	12:18:19.2 x +25:35:34	29.33	3.472	5
229090	12:36:44.1 x +33:36:44	12:36:54.6 x +33:36:50	87.45	2.192	5
229284	12:17:18.0 x +28:35:09	12:17:11.1 x +28:37:21	145.59	2.661	5
229379	12:30:37.3 x +23:11:41	12:30:30.9 x +23:12:57	130.94	1.937	5
229439	12:51:36.3 x +32:10:09	12:51:43.2 x +32:11:31	47.00	2.002	5
238890	13:32:32.6 x +25:06:47	13:32:27.6 x +25:08:01	137.48	1.678	5
239031	13:08:14.7 x +29:04:37	13:08:09.5 x +29.06.03	141.33	1.837	5
322463	22:59:32.9 x +16:45:15	22:59:38.3 x +16:46:36	43.810	1.871	5
724906	12:30:58.9 x +26:29:46	12:30:50.4 x +26:31:43	135.87	2.728	5
728909	13:22:27.5 x +35:11:36	13:22:27.7 x +35:13:02	1.10	1.430	5
732041	12:17:46.6 x +27:27:56	12:17:38.4 x +27:30:05	139.52	2.834	5
732129	12:27:28.0 x +27:49:52	12:27:21.9 x +27:51:13	135.43	1.910	5
732226	12:40:48.7 x +25:55:45	12:40:48.0 x +25:57:41	175.60	1.934	5
732418	12:59:06.8 x +26:21:54	12:59:08.7 x +26:23:18	17.06	1.452	5
742601	12:49:30.0 x +21:55:01	12:49:44.7 x +21:55:04	89.30	3.409	5

Table 5. Overview: Masses

Galaxy AGC	HI Mass ($M_\odot$)	Stellar Mass ($M_\odot$)	Dynamic Mass ($M_\odot$)	Dark Matter Mass ($M_\odot$)	Percentage of Dark Matter (%)
221089	1.40E+07		1.28E+08	1.14E+08	89.05
223231	1.58E+07	5.62E+06	1.44E+08	1.22E+08	85.07
223254	1.12E+07		6.51E+07	5.38E+07	82.74
229052	1.08E+07		4.82E+07	3.74E+07	77.50
229053	2.83E+07	8.91E+06	3.52E+08	3.15E+08	89.43
229090	1.34E+07		1.50E+08	1.37E+08	91.06
229284	1.12E+07		8.12E+07	6.99E+07	86.15
229379	5.05E+06		3.81E+07	3.31E+07	86.75
229439	1.37E+07		2.15E+08	2.01E+08	93.63
238890	2.35E+06		2.71E+07	2.47E+07	91.32
239031	1.29E+07		9.83E+07	8.55E+07	86.91
322463	8.96E+06		5.86E+07	4.97E+07	84.72
724906	1.52E+07		1.26E+08	1.10E+08	87.89
728909	1.35E+07		7.04E+07	5.70E+07	80.86
732041	5.98E+06		1.04E+08	9.78E+07	94.23
732129	1.08E+07		8.39E+07	7.31E+07	87.13
732226	1.22E+07		6.85E+07	5.63E+07	82.17
732418	5.50E+06		3.28E+07	2.73E+07	83.21
742601	1.02E+07	4.37E+06	1.48E+08	1.33E+08	90.19

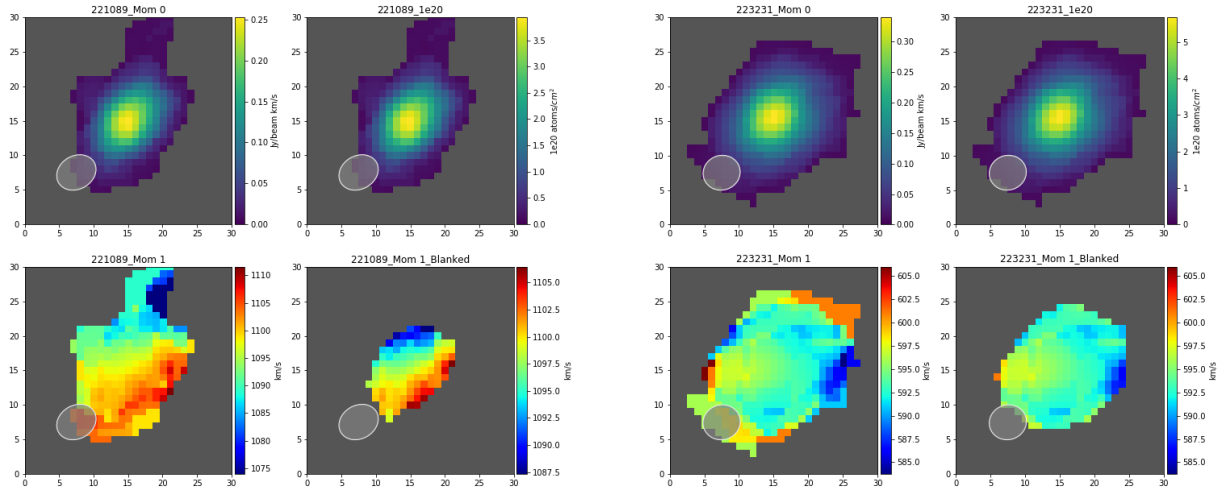

Figure 1. (Left) AGC221089 - Top Left, Moment 0 map; Top Right, $1e^{20}$ map; Bottom Left, Moment 1 map; Bottom Left, Blanked Moment 1 map. The abscissa and the ordinate axes are in units of pixels, with the central pixels being the right ascension and declination of the galaxy.(Right) AGC223231 - Top Left, Moment 0 map; Top Right, $1e^{20}$ map; Bottom Left, Moment 1 map; Bottom Left, Blanked Moment 1 map. The abscissa and the ordinate axes are in units of pixels, with the central pixels being the right ascension and declination of the galaxy.

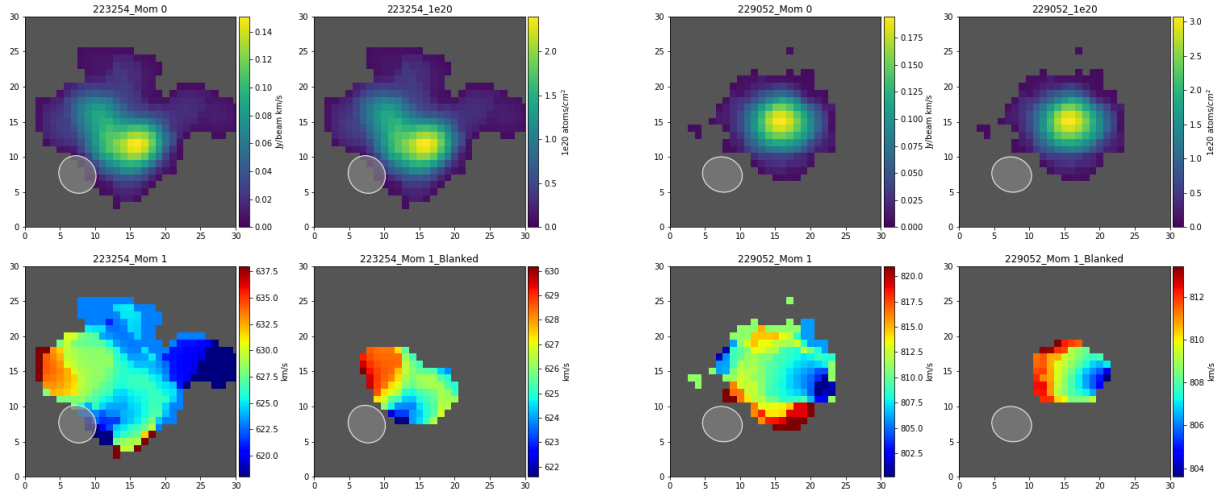

Figure 2. (Left) AGC223254 - Top Left, Moment 0 map; Top Right, $1e^{20}$ map; Bottom Left, Moment 1 map; Bottom Left, Blanked Moment 1 map. The abscissa and the ordinate axes are in units of pixels, with the central pixels being the right ascension and declination of the galaxy.(Right) AGC229052 - Top Left, Moment 0 map; Top Right, $1e^{20}$ map; Bottom Left, Moment 1 map; Bottom Left, Blanked Moment 1 map. The abscissa and the ordinate axes are in units of pixels, with the central pixels being the right ascension and declination of the galaxy.

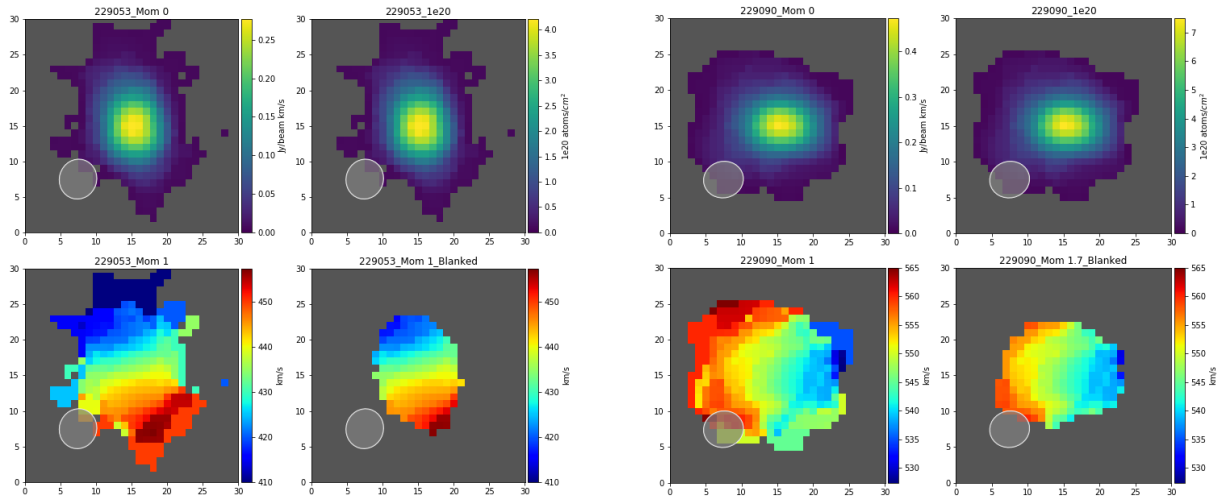

Figure 3. (Left) AGC229053 - Top Left, Moment 0 map; Top Right, $1e^{20}$ map; Bottom Left, Moment 1 map; Bottom Left, Blanked Moment 1 map. The abscissa and the ordinate axes are in units of pixels, with the central pixels being the right ascension and declination of the galaxy.(Right) AGC229090 - Top Left, Moment 0 map; Top Right, $1e^{20}$ map; Bottom Left, Moment 1 map; Bottom Left, Blanked Moment 1 map. The abscissa and the ordinate axes are in units of pixels, with the central pixels being the right ascension and declination of the galaxy.

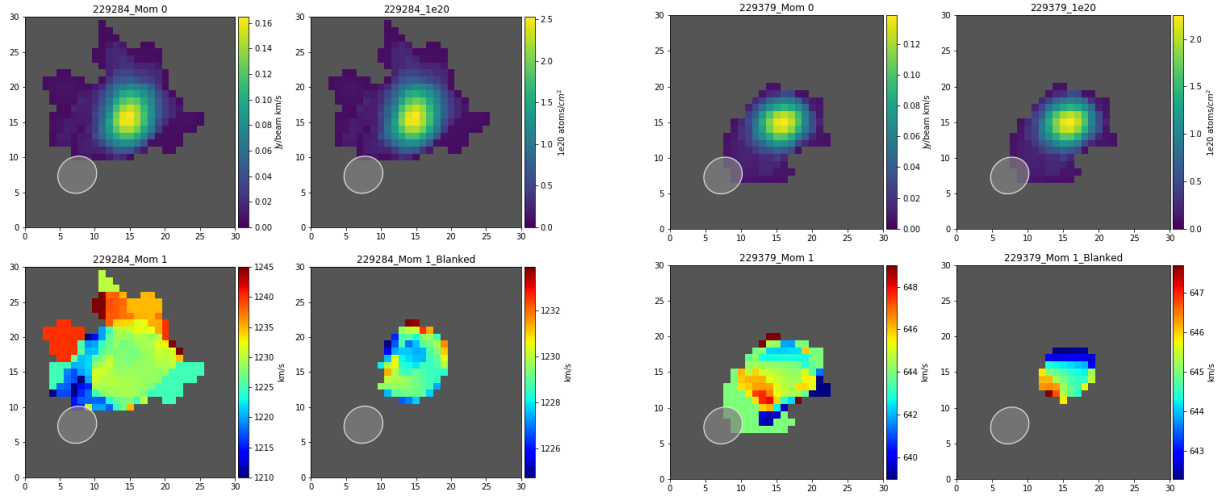

Figure 4. (Left) AGC229284 - Top Left, Moment 0 map; Top Right, $1e^{20}$ map; Bottom Left, Moment 1 map; Bottom Left, Blanked Moment 1 map. The abscissa and the ordinate axes are in units of pixels, with the central pixels being the right ascension and declination of the galaxy.(Right) AGC229379 - Top Left, Moment 0 map; Top Right, $1e^{20}$ map; Bottom Left, Moment 1 map; Bottom Left, Blanked Moment 1 map. The abscissa and the ordinate axes are in units of pixels, with the central pixels being the right ascension and declination of the galaxy.

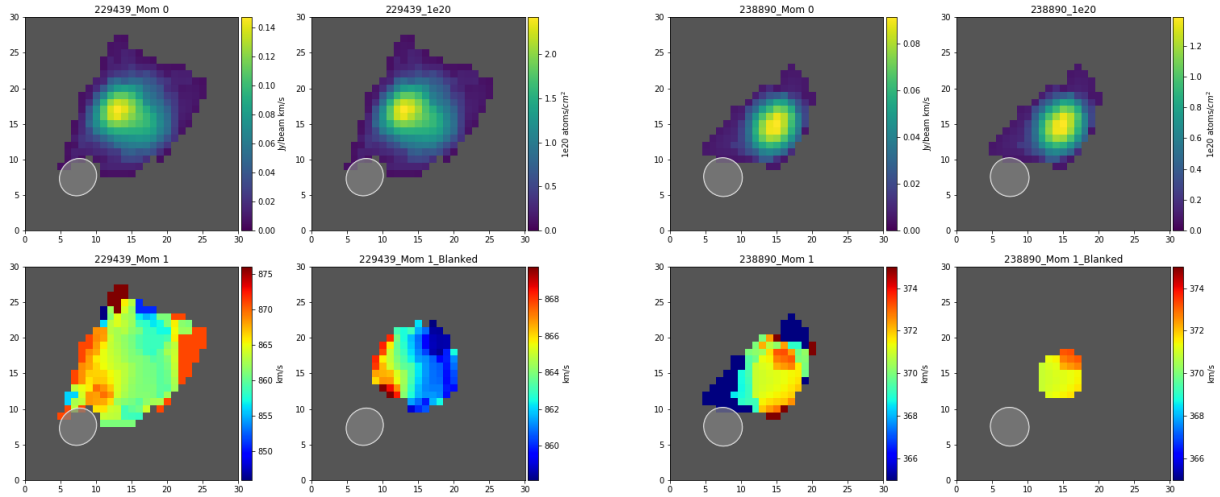

Figure 5. (Left) AGC229439 - Top Left, Moment 0 map; Top Right, $1e^{20}$ map; Bottom Left, Moment 1 map; Bottom Left, Blanked Moment 1 map. The abscissa and the ordinate axes are in units of pixels, with the central pixels being the right ascension and declination of the galaxy.(Right) AGC238890 - Top Left, Moment 0 map; Top Right, $1e^{20}$ map; Bottom Left, Moment 1 map; Bottom Left, Blanked Moment 1 map. The abscissa and the ordinate axes are in units of pixels, with the central pixels being the right ascension and declination of the galaxy.

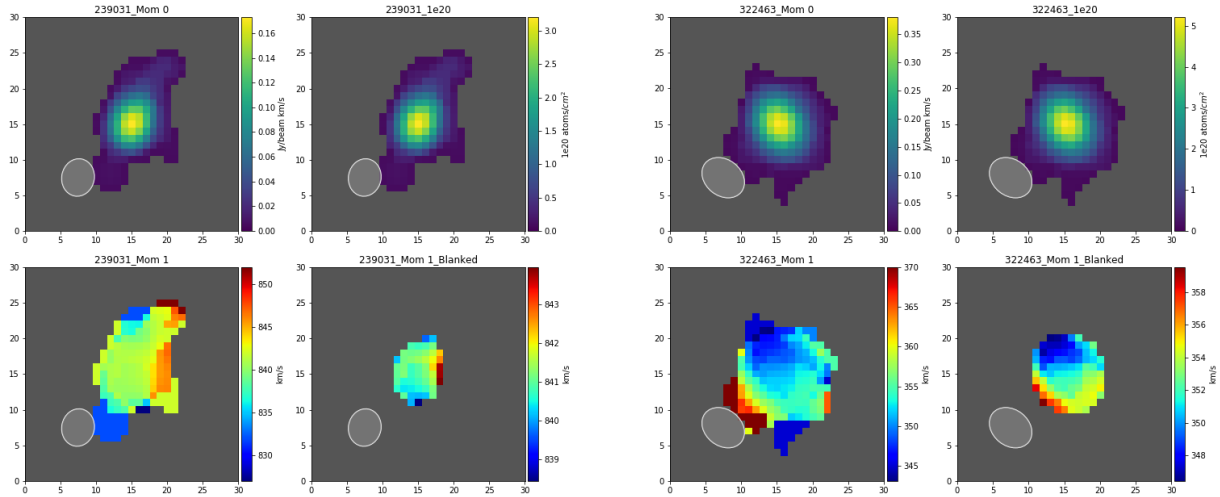

Figure 6. (Left) AGC239031 - Top Left, Moment 0 map; Top Right, $1e^{20}$ map; Bottom Left, Moment 1 map; Bottom Left, Blanked Moment 1 map. The abscissa and the ordinate axes are in units of pixels, with the central pixels being the right ascension and declination of the galaxy.(Right) AGC322463 - Top Left, Moment 0 map; Top Right, $1e^{20}$ map; Bottom Left, Moment 1 map; Bottom Left, Blanked Moment 1 map. The abscissa and the ordinate axes are in units of pixels, with the central pixels being the right ascension and declination of the galaxy.

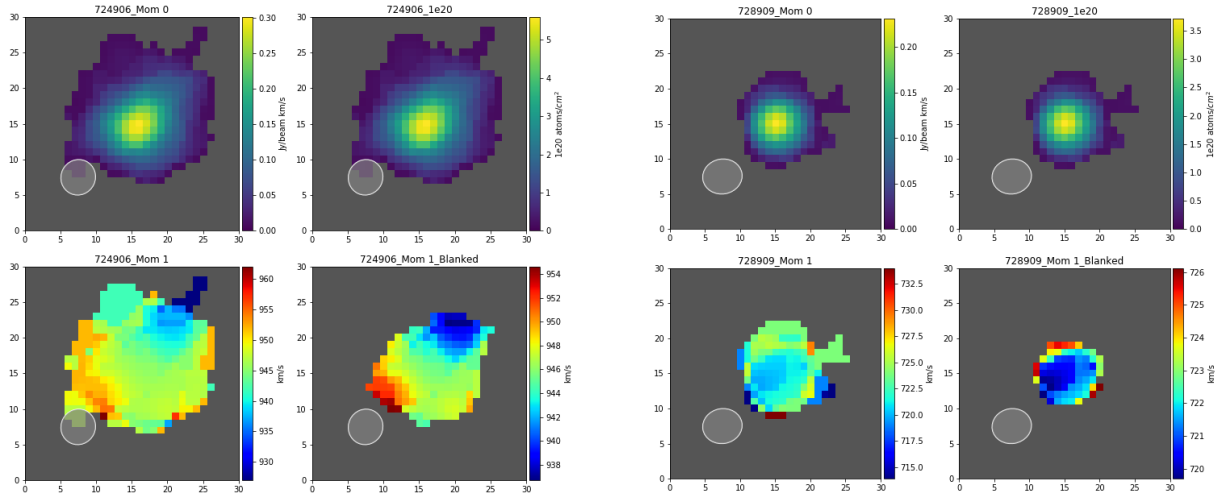

Figure 7. (Left) AGC724906 - Top Left, Moment 0 map; Top Right, $1e^{20}$ map; Bottom Left, Moment 1 map; Bottom Left, Blanked Moment 1 map. The abscissa and the ordinate axes are in units of pixels, with the central pixels being the right ascension and declination of the galaxy.(Right) AGC728909 - Top Left, Moment 0 map; Top Right, $1e^{20}$ map; Bottom Left, Moment 1 map; Bottom Left, Blanked Moment 1 map. The abscissa and the ordinate axes are in units of pixels, with the central pixels being the right ascension and declination of the galaxy.

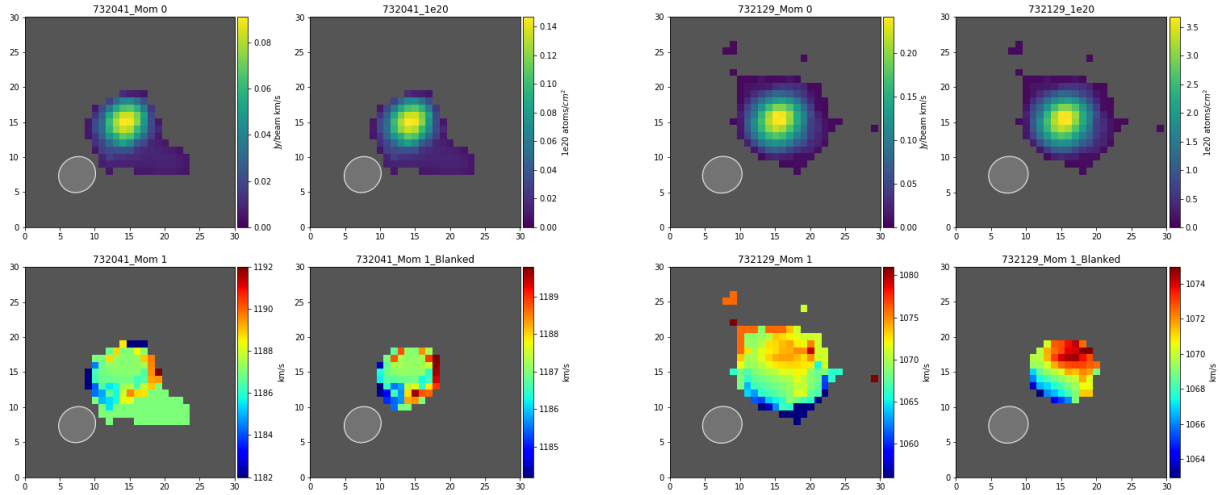

Figure 8. (Left) AGC732041 - Top Left, Moment 0 map; Top Right, $1e^{20}$ map; Bottom Left, Moment 1 map; Bottom Left, Blanked Moment 1 map. The abscissa and the ordinate axes are in units of pixels, with the central pixels being the right ascension and declination of the galaxy.(Right) AGC732129 - Top Left, Moment 0 map; Top Right, $1e^{20}$ map; Bottom Left, Moment 1 map; Bottom Left, Blanked Moment 1 map. The abscissa and the ordinate axes are in units of pixels, with the central pixels being the right ascension and declination of the galaxy.

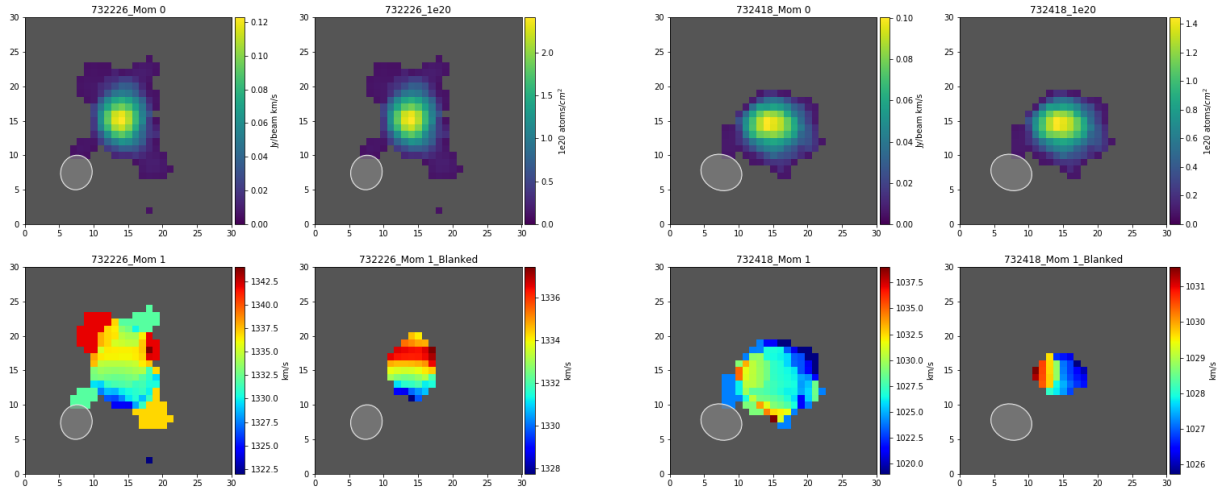

Figure 9. (Left) AGC732226 - Top Left, Moment 0 map; Top Right, $1e^{20}$ map; Bottom Left, Moment 1 map; Bottom Left, Blanked Moment 1 map. The abscissa and the ordinate axes are in units of pixels, with the central pixels being the right ascension and declination of the galaxy.(Right) AGC732418 - Top Left, Moment 0 map; Top Right, $1e^{20}$ map; Bottom Left, Moment 1 map; Bottom Left, Blanked Moment 1 map. The abscissa and the ordinate axes are in units of pixels, with the central pixels being the right ascension and declination of the galaxy.

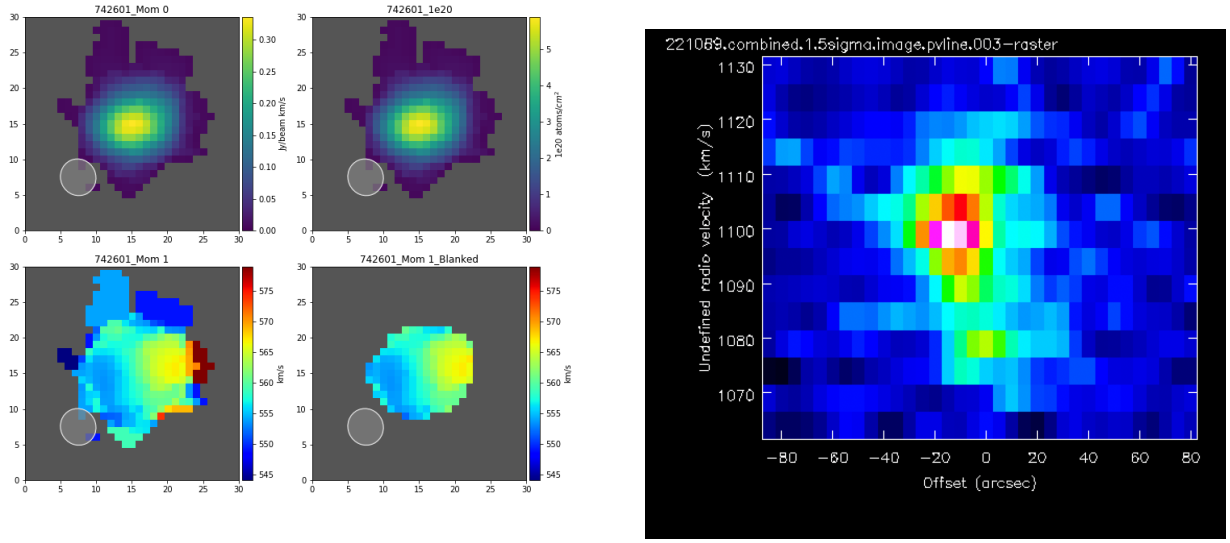

Figure 10. (Left) AGC742601 - Top Left, Moment 0 map; Top Right, $1e^{20}$ map; Bottom Left, Moment 1 map; Bottom Left, Blanked Moment 1 map. The abscissa and the ordinate axes are in units of pixels, with the central pixels being the right ascension and declination of the galaxy.(Right) AGC221089 - Position-Velocity slice: Offset (arcseconds) vs Radio Velocity (km/s), gradient is HI column density (red, more dense; blue, less dense)

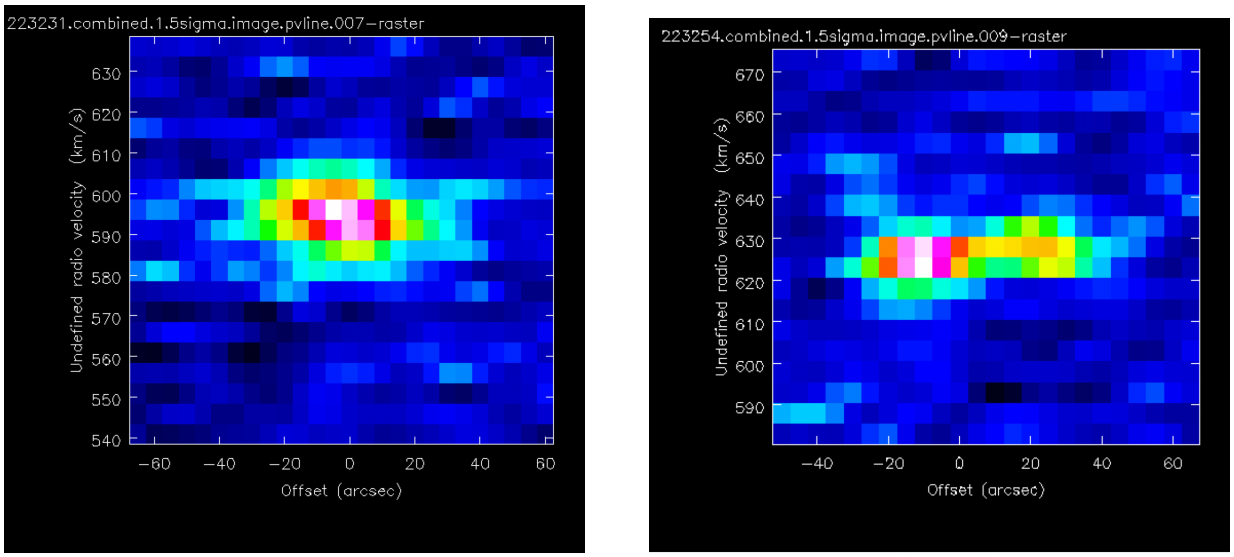

Figure 11. (Left) AGC223231 - Position-Velocity slice: Offset (arcseconds) vs Radio Velocity (km/s), gradient is HI column density (red, more dense; blue, less dense). (Right) AGC223254 - Position-Velocity slice: Offset (arcseconds) vs Radio Velocity (km/s), gradient is HI column density (red, more dense; blue, less dense).

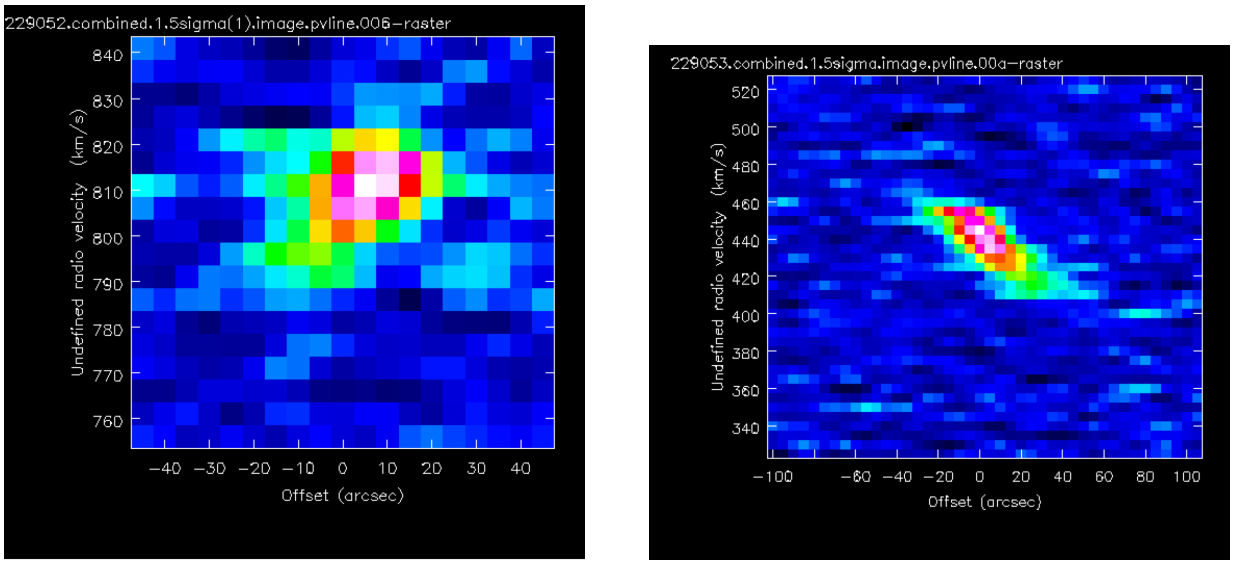

Figure 12. (Left) AGC2290521 - Position-Velocity slice: Offset (arcseconds) vs Radio Velocity (km/s), gradient is HI column density (red, more dense; blue, less dense). (Right) AGC229053 - Position-Velocity slice: Offset (arcseconds) vs Radio Velocity (km/s), gradient is HI column density (red, more dense; blue, less dense).

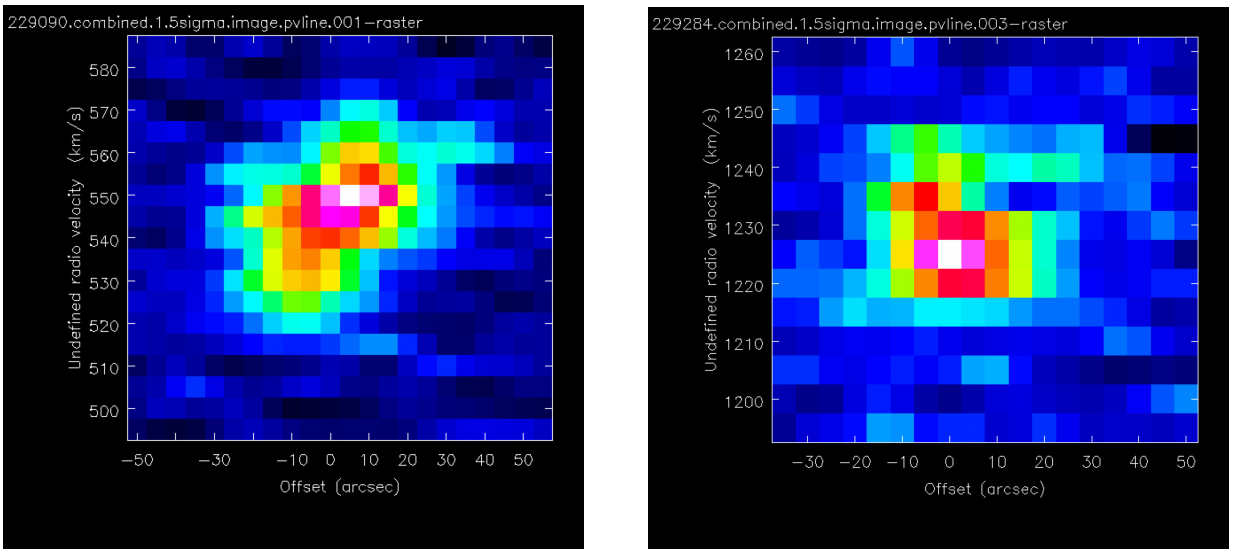

Figure 13. (Left) AGC229090 - Position-Velocity slice: Offset (arcseconds) vs Radio Velocity (km/s), gradient is HI column density (red, more dense; blue, less dense). (Right) AGC229284 - Position-Velocity slice: Offset (arcseconds) vs Radio Velocity (km/s), gradient is HI column density (red, more dense; blue, less dense).

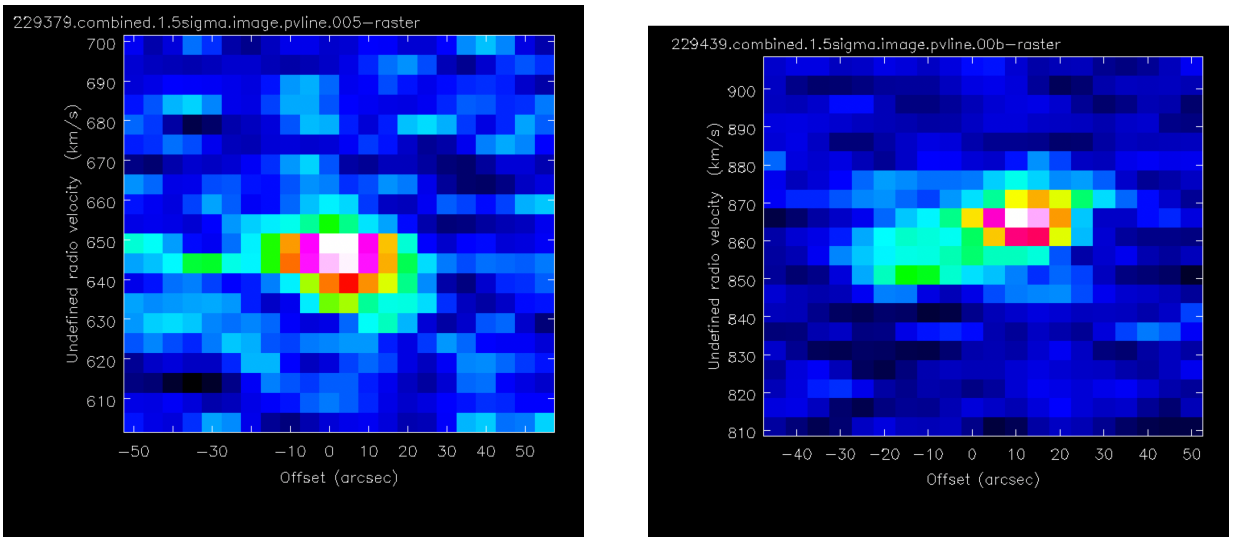

Figure 14. (Left) AGC229379 - Position-Velocity slice: Offset (arcseconds) vs Radio Velocity (km/s), gradient is HI column density (red, more dense; blue, less dense). (Right) AGC229439 - Position-Velocity slice: Offset (arcseconds) vs Radio Velocity (km/s), gradient is HI column density (red, more dense; blue, less dense).

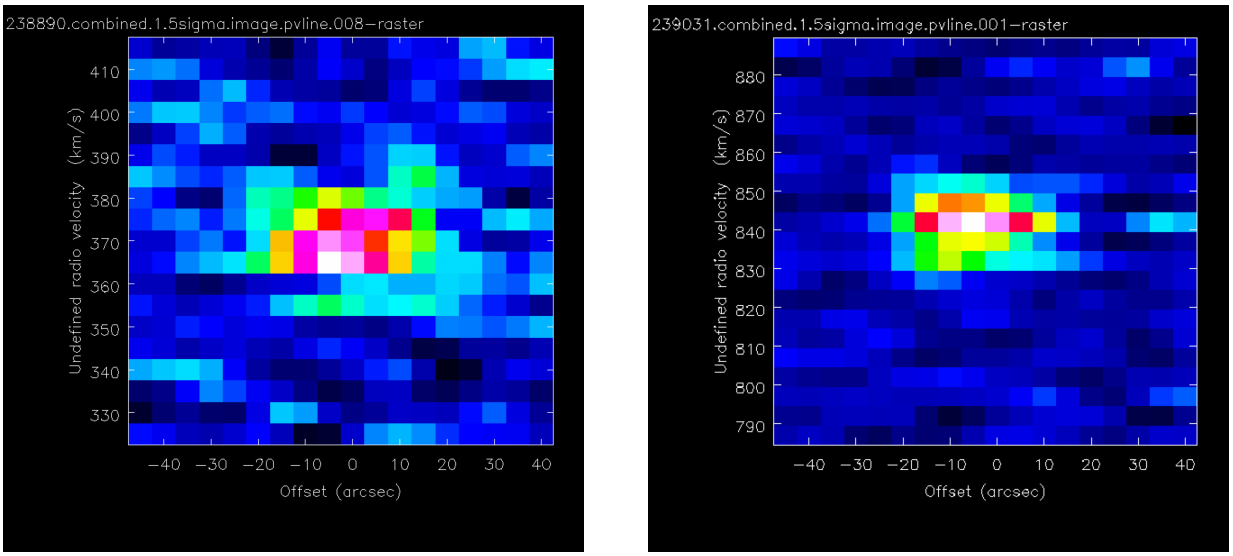

Figure 15. (Left) AGC238890 - Position-Velocity slice: Offset (arcseconds) vs Radio Velocity (km/s), gradient is HI column density (red, more dense; blue, less dense). (Right) AGC239031 - Position-Velocity slice: Offset (arcseconds) vs Radio Velocity (km/s), gradient is HI column density (red, more dense; blue, less dense).

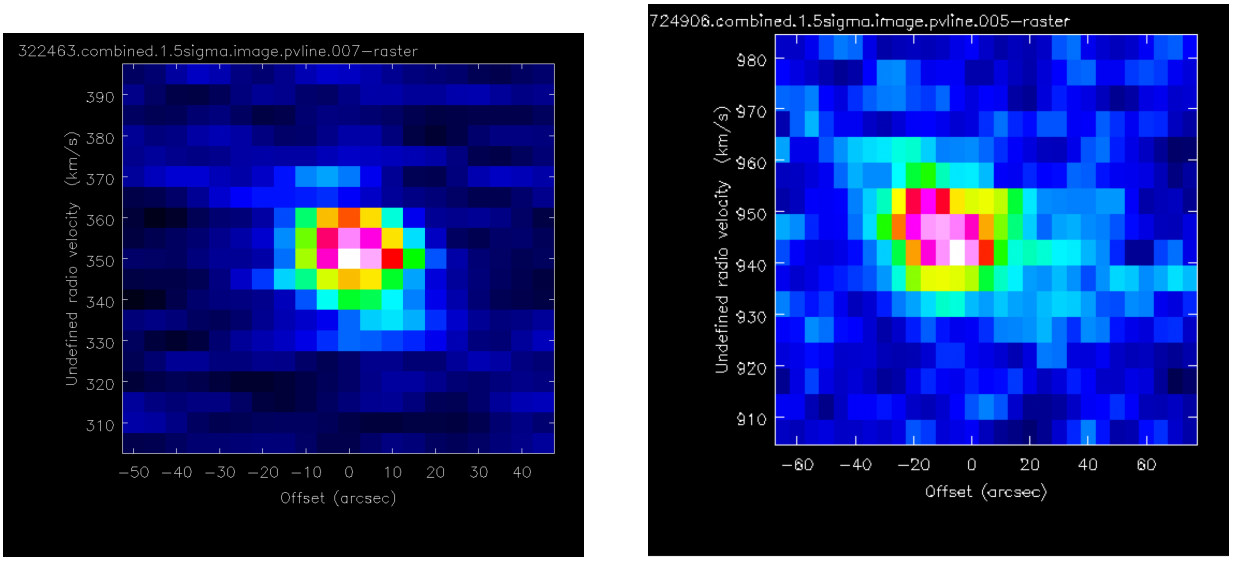

Figure 16. (Left) AGC322463 - Position-Velocity slice: Offset (arcseconds) vs Radio Velocity (km/s), gradient is HI column density (red, more dense; blue, less dense). (Right) AGC724906 - Position-Velocity slice: Offset (arcseconds) vs Radio Velocity (km/s), gradient is HI column density (red, more dense; blue, less dense).

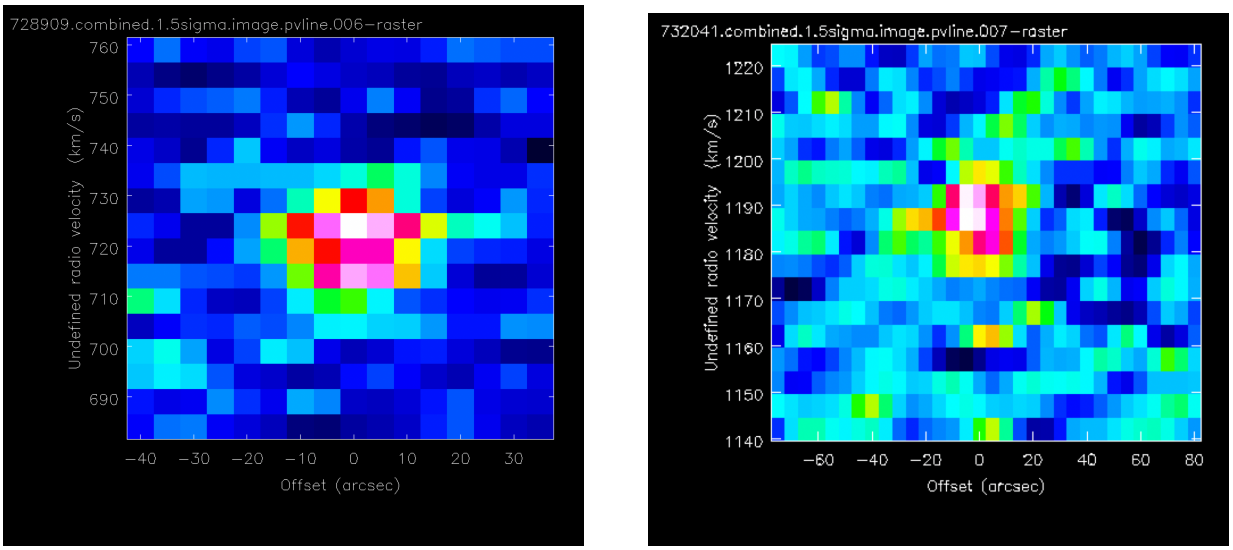

Figure 17. (Left) AGC728909 - Position-Velocity slice: Offset (arcseconds) vs Radio Velocity (km/s), gradient is HI column density (red, more dense; blue, less dense). (Right) AGC732041 - Position-Velocity slice: Offset (arcseconds) vs Radio Velocity (km/s), gradient is HI column density (red, more dense; blue, less dense).

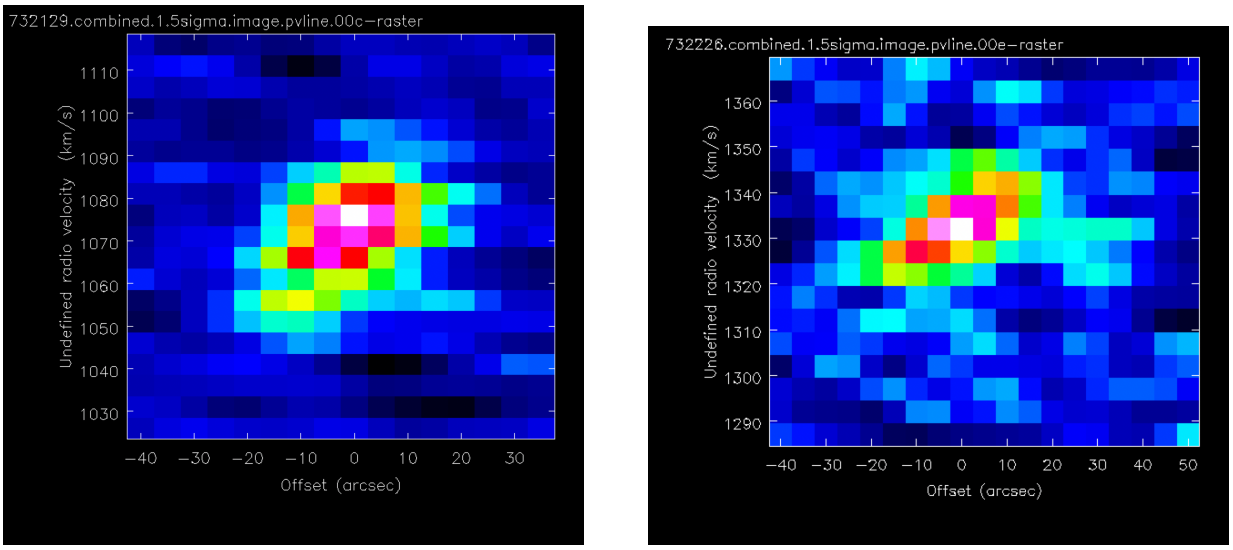

Figure 18. (Left) AGC732129 - Position-Velocity slice: Offset (arcseconds) vs Radio Velocity (km/s), gradient is HI column density (red, more dense; blue, less dense). (Right) AGC732226 - Position-Velocity slice: Offset (arcseconds) vs Radio Velocity (km/s), gradient is HI column density (red, more dense; blue, less dense).

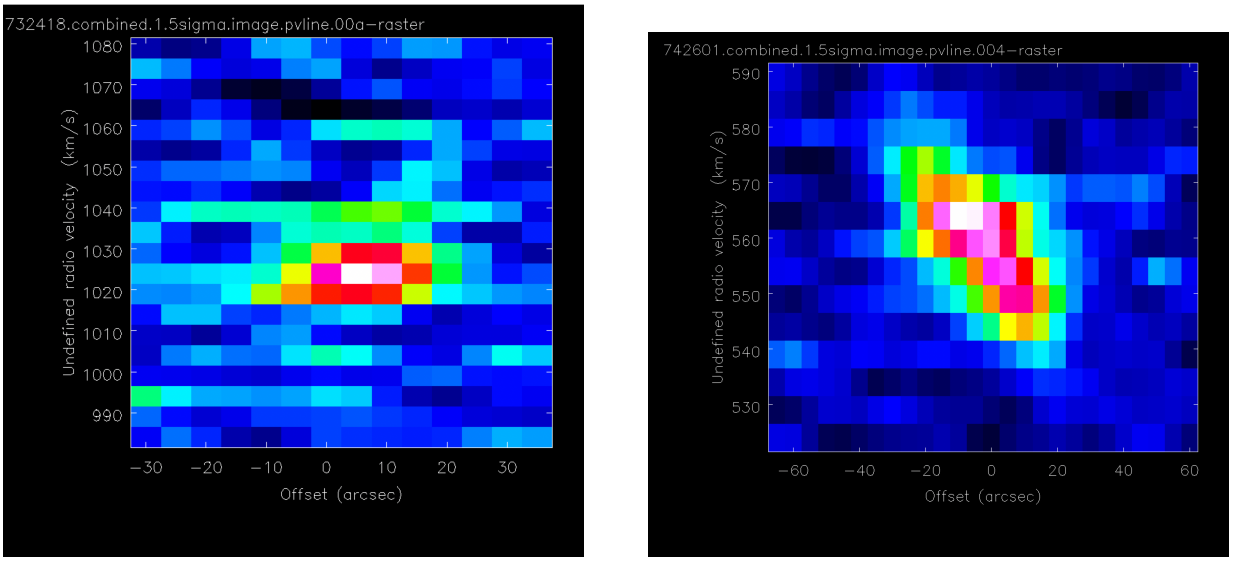

Figure 19. (Left) AGC732418 - Position-Velocity slice: Offset (arcseconds) vs Radio Velocity (km/s), gradient is HI column density (red, more dense; blue, less dense). (Right) AGC742601 - Position-Velocity slice: Offset (arcseconds) vs Radio Velocity (km/s), gradient is HI column density (red, more dense; blue, less dense).

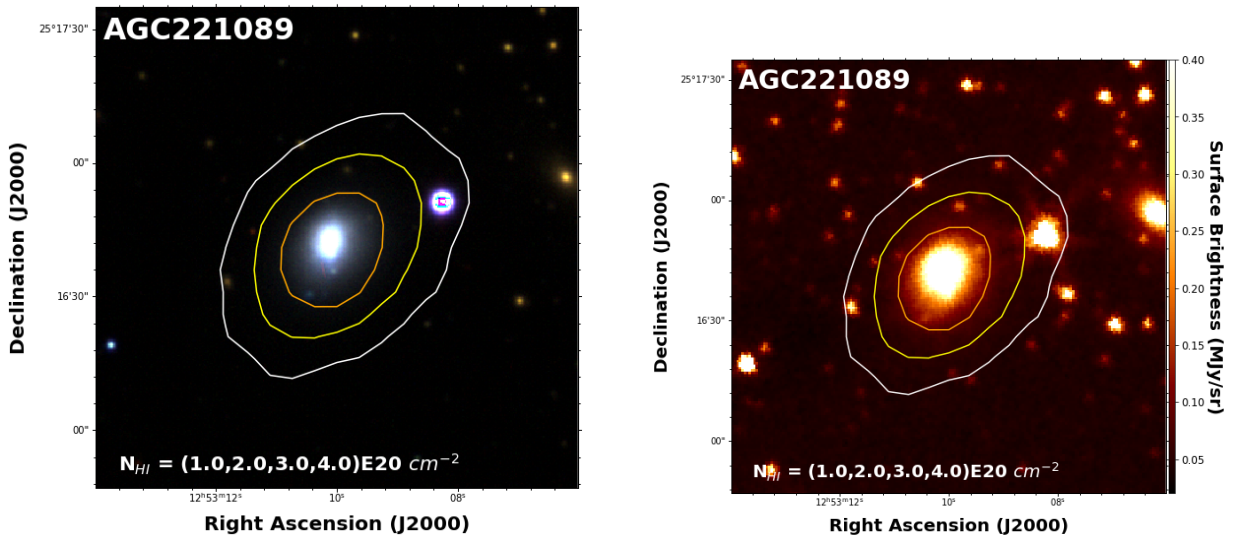

Figure 20. AGC 221089 (Left) three color Legacy Survey image with $1e^{20}$ contour overlay. (Right) Spitzer 3.6 µm image with moment $1e^{20}$ overlay

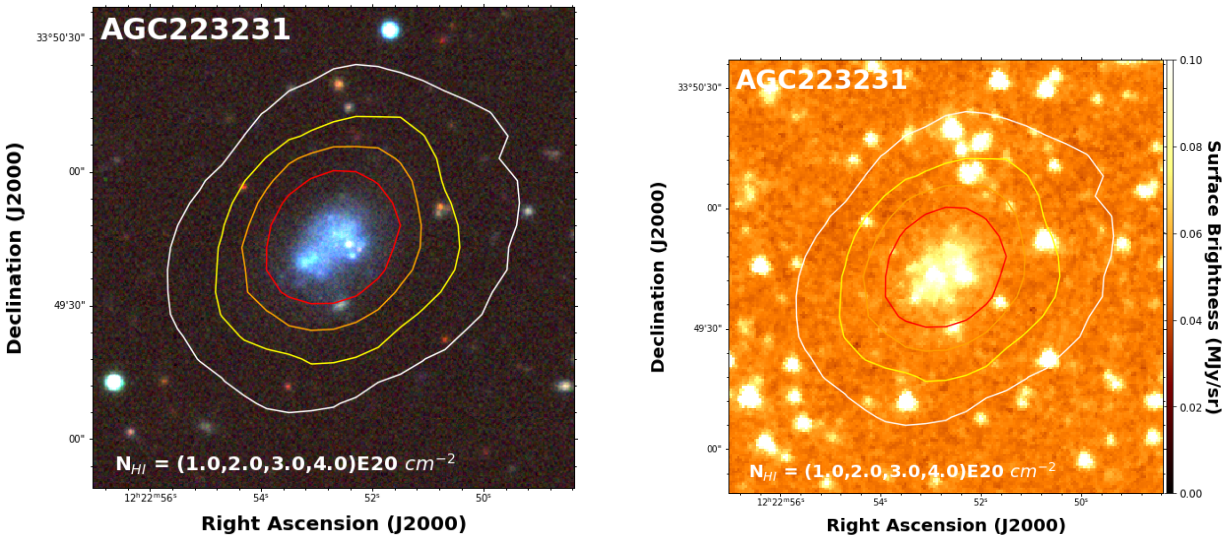

Figure 21. AGC 223231 (Left) three color Legacy Survey image with $1e^{20}$ contour overlay. (Right) Spitzer 3.6 µm image with moment $1e^{20}$ overlay

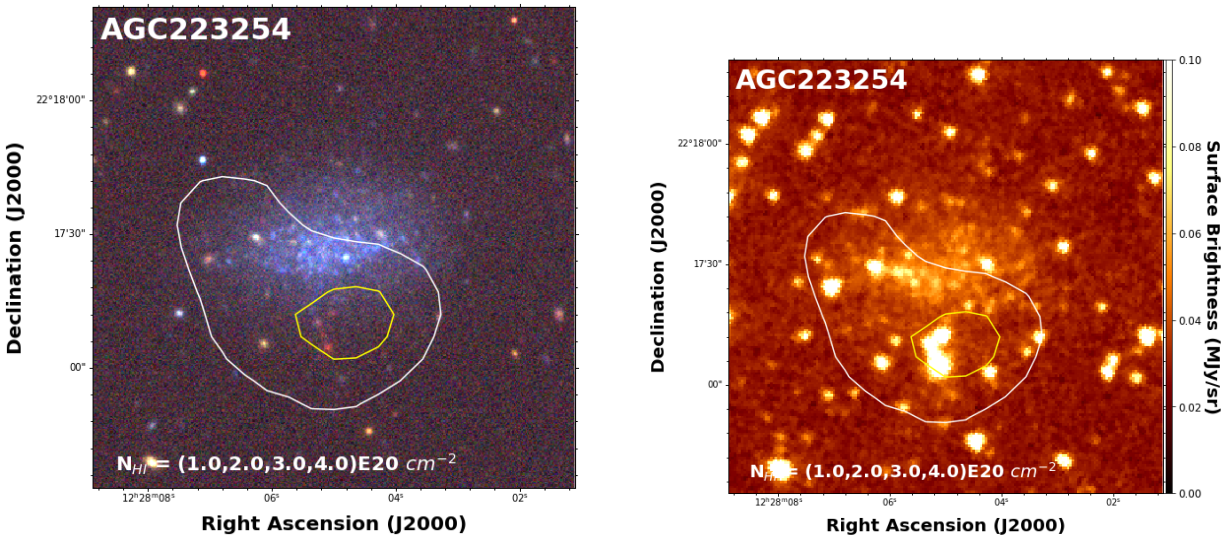

Figure 22. AGC 223254 (Left) three color Legacy Survey image with $1e^{20}$ contour overlay. (Right) Spitzer 3.6 µm image with moment $1e^{20}$ overlay

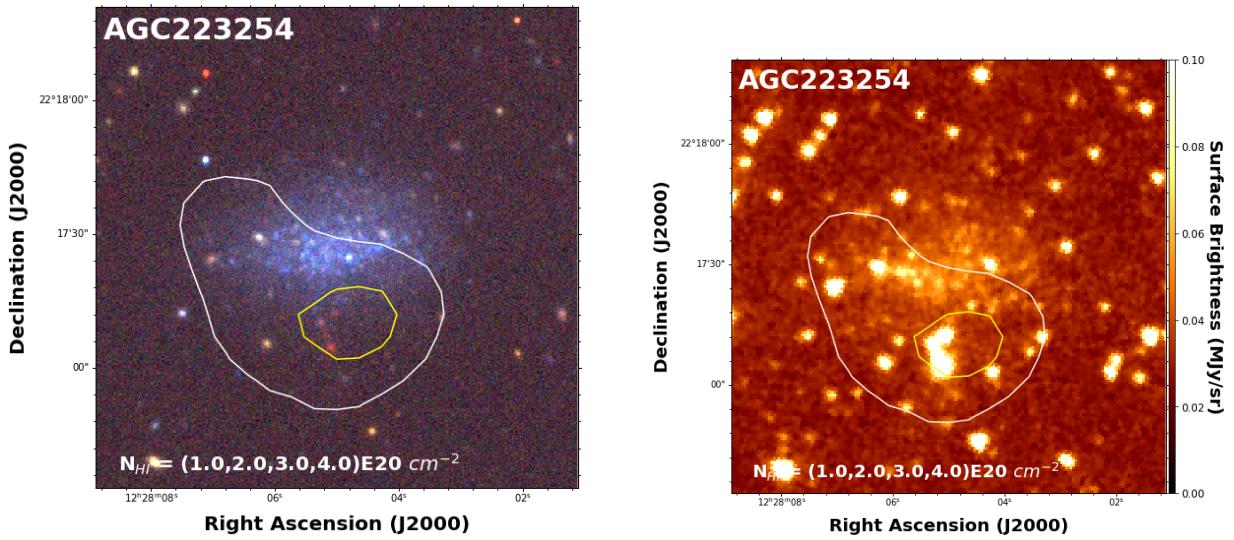

Figure 23. AGC 223254 (Left) three color Legacy Survey image with $1e^{20}$ contour overlay. (Right) Spitzer 3.6 µm image with moment $1e^{20}$ overlay

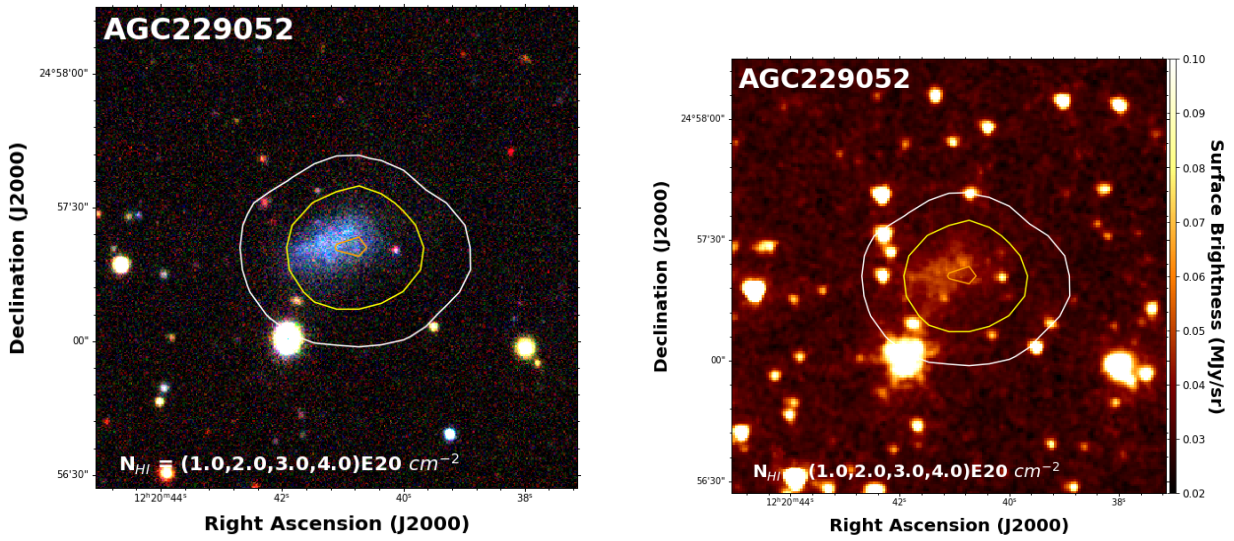

Figure 24. AGC 229052 (Left) three color Legacy Survey image with $1e^{20}$ contour overlay. (Right) Spitzer 3.6 µm image with moment $1e^{20}$ overlay

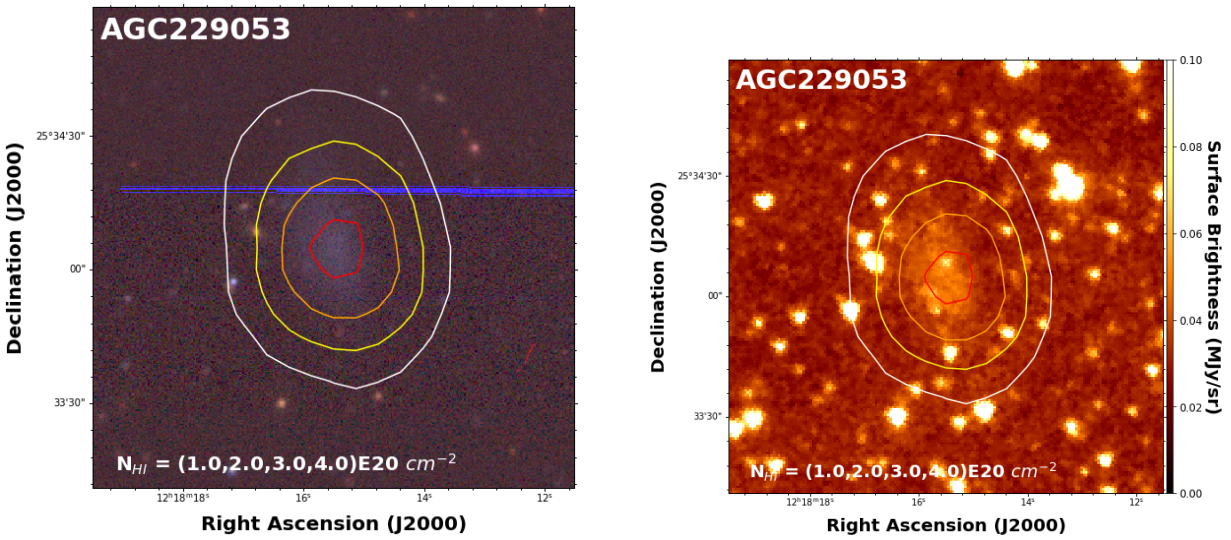

Figure 25. AGC 229053 (Left) three color Legacy Survey image with $1e^{20}$ contour overlay. (Right) Spitzer 3.6 µm image with moment $1e^{20}$ overlay

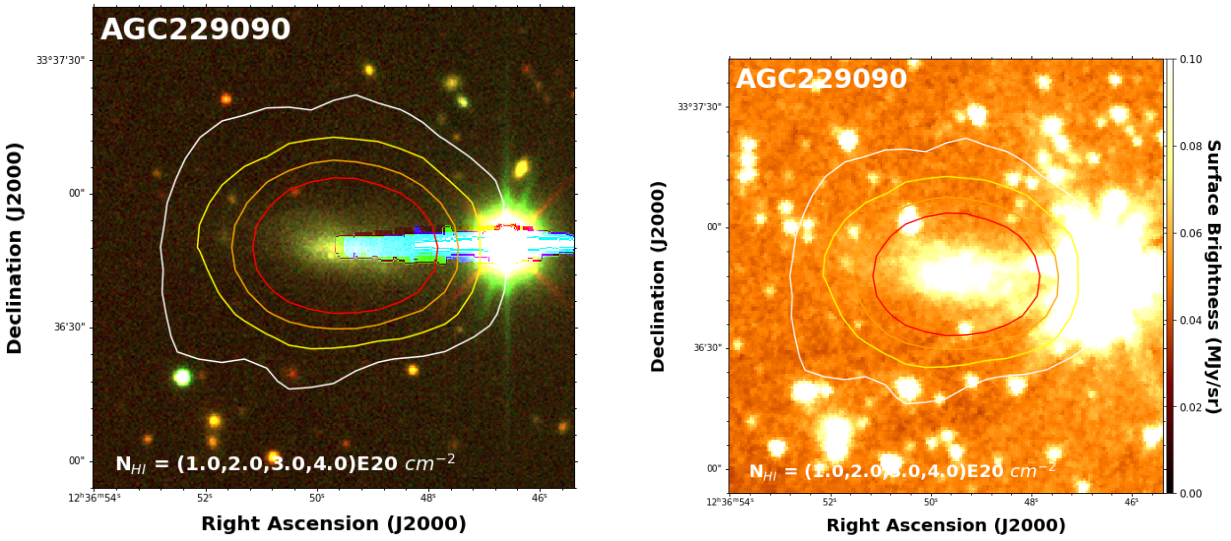

Figure 26. AGC 229090 (Left) three color Legacy Survey image with $1e^{20}$ contour overlay. (Right) Spitzer 3.6 µm image with moment $1e^{20}$ overlay

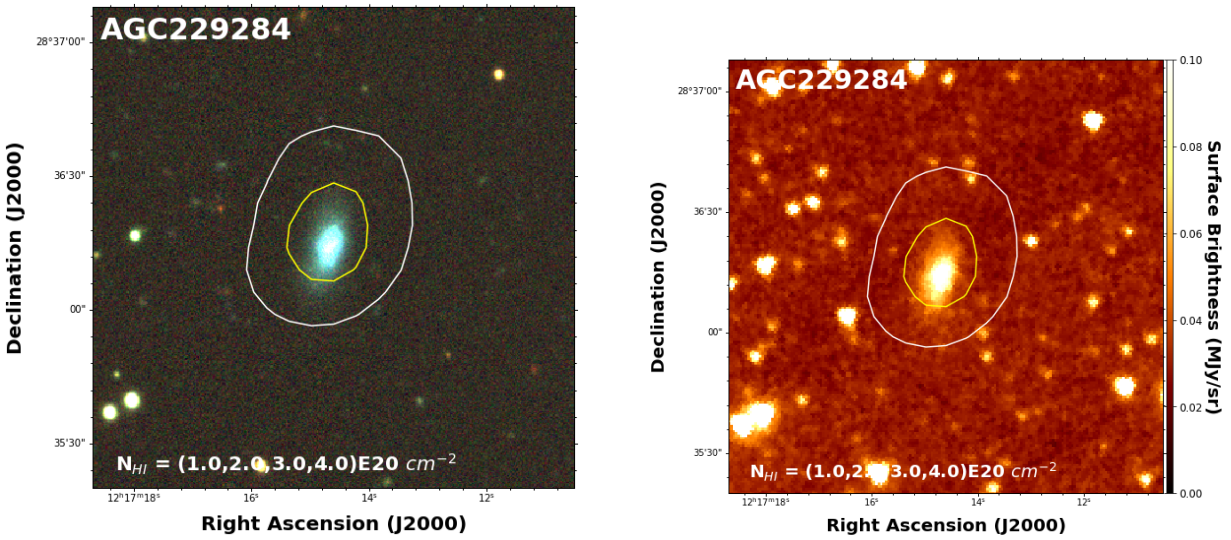

Figure 27. AGC 229284 (Left) three color Legacy Survey image with $1e^{20}$ contour overlay. (Right) Spitzer 3.6 µm image with moment $1e^{20}$ overlay

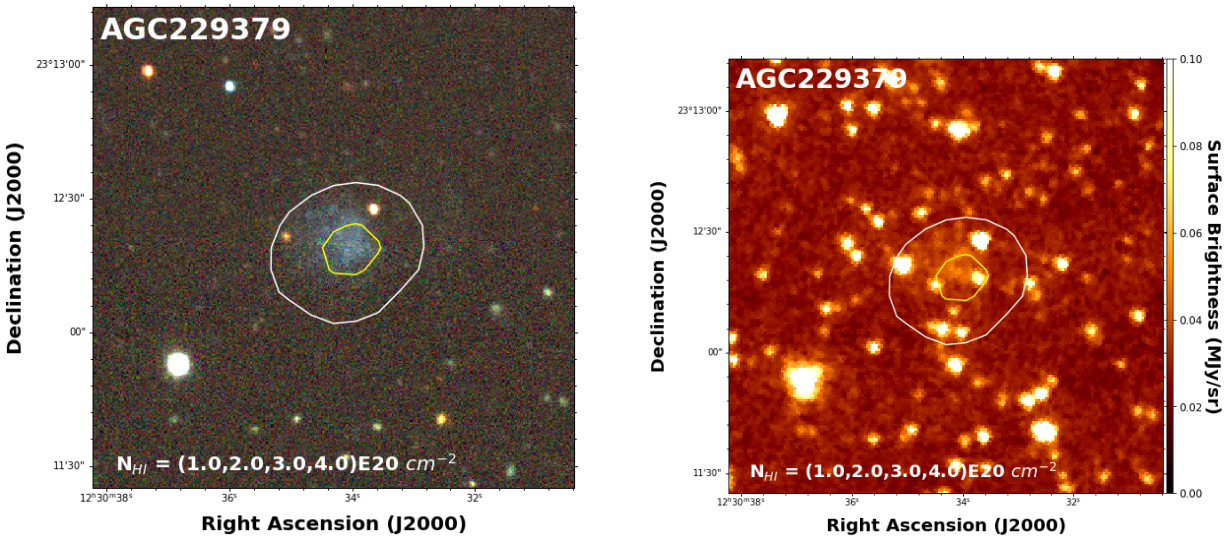

Figure 28. AGC 229379 (Left) three color Legacy Survey image with $1e^{20}$ contour overlay. (Right) Spitzer 3.6 µm image with moment $1e^{20}$ overlay

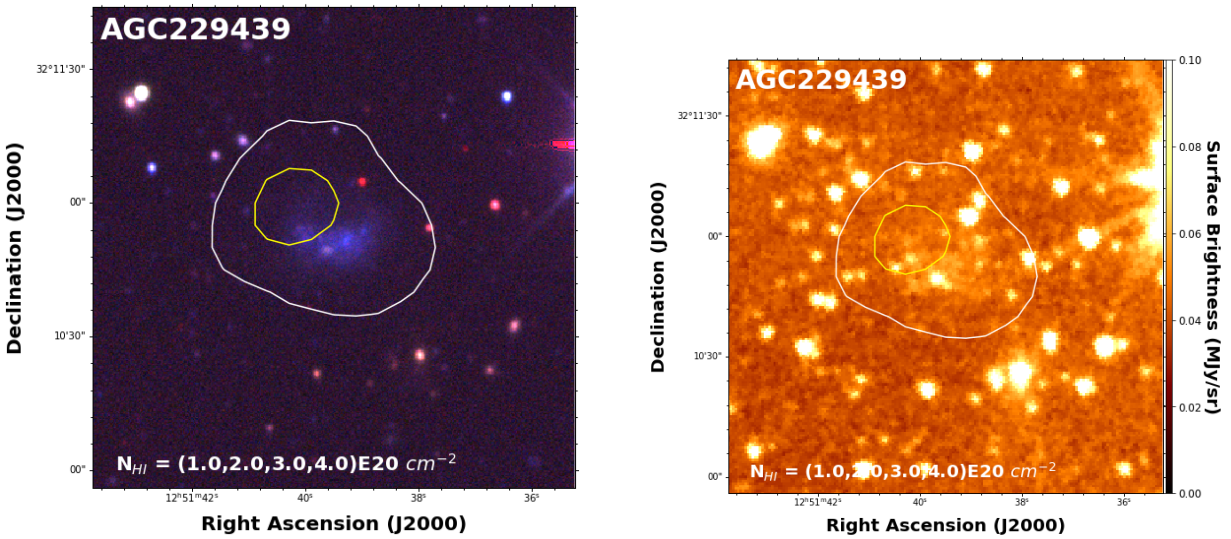

Figure 29. AGC 229439 (Left) three color Legacy Survey image with $1e^{20}$ contour overlay. (Right) Spitzer 3.6 µm image with moment $1e^{20}$ overlay

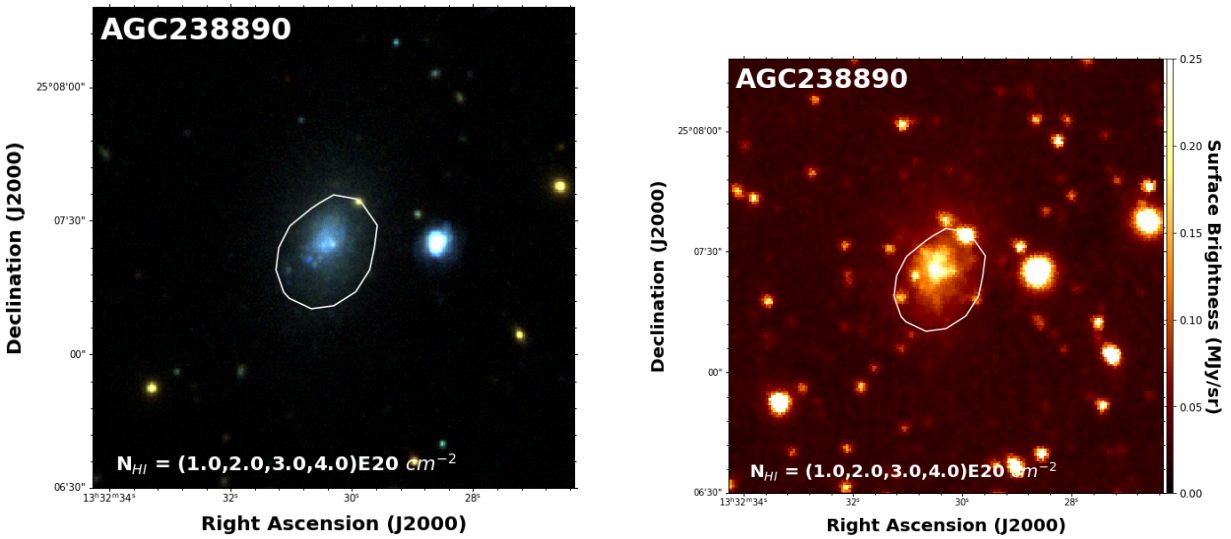

Figure 30. AGC 238890 (Left) three color Legacy Survey image with $1e^{20}$ contour overlay. (Right) Spitzer 3.6 µm image with moment $1e^{20}$ overlay

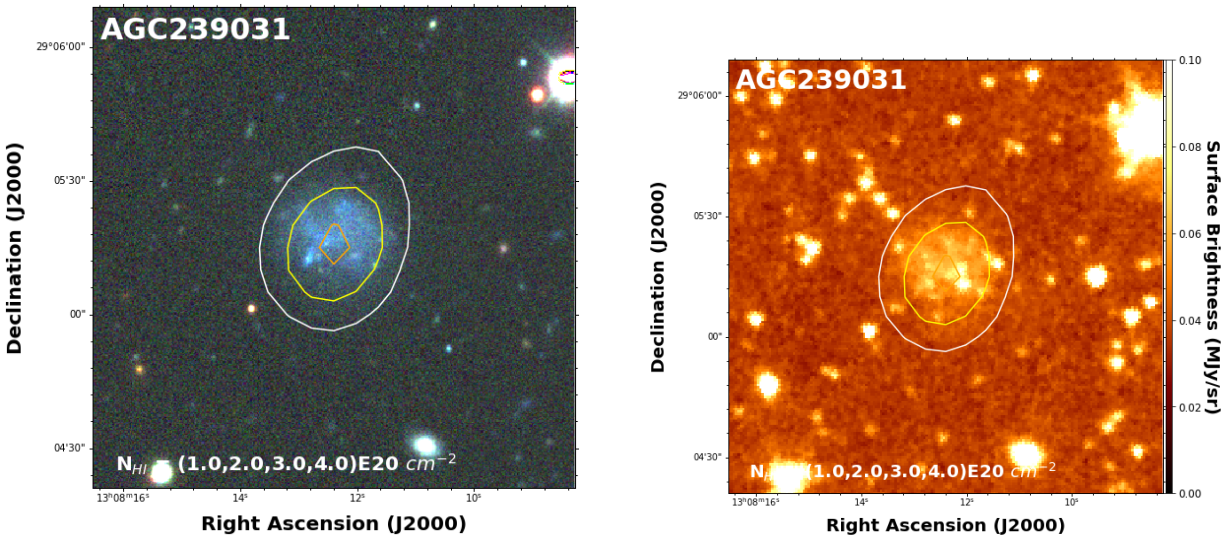

Figure 31. AGC 239031 (Left) three color Legacy Survey image with $1e^{20}$ contour overlay. (Right) Spitzer 3.6 µm image with moment $1e^{20}$ overlay

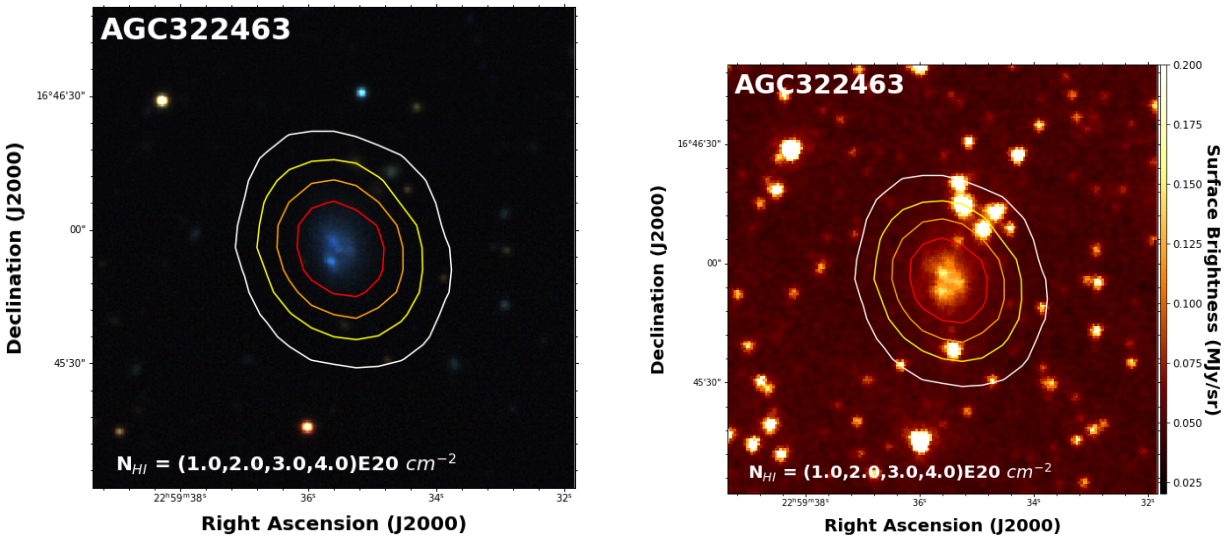

Figure 32. AGC 322463 (Left) three color Legacy Survey image with $1e^{20}$ contour overlay. (Right) Spitzer 3.6 µm image with moment $1e^{20}$ overlay

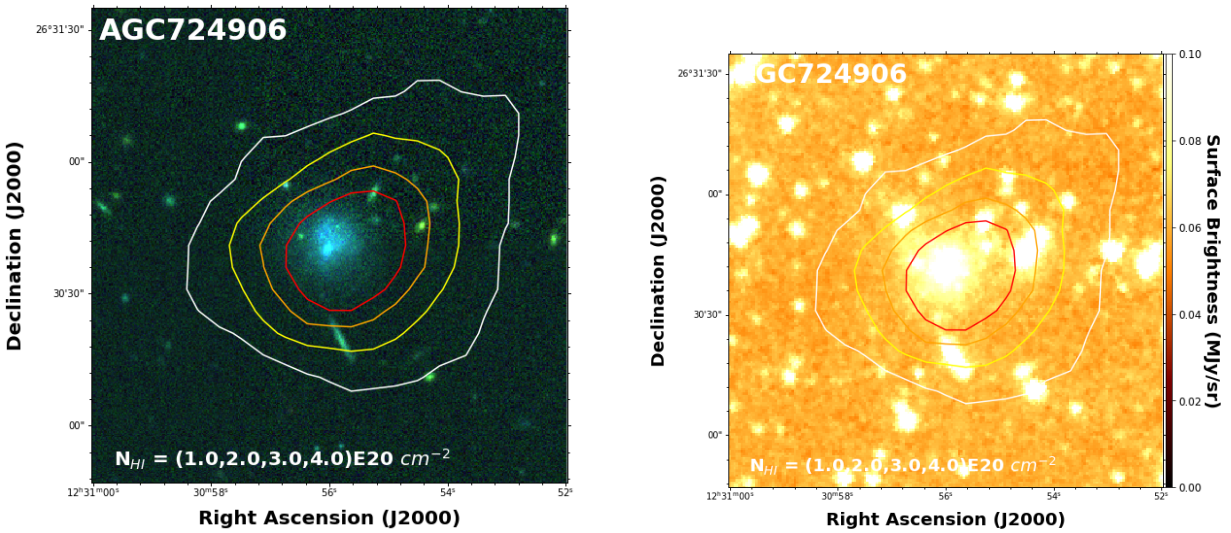

Figure 33. AGC 724906 (Left) three color Legacy Survey image with $1e^{20}$ contour overlay. (Right) Spitzer 3.6 µm image with moment $1e^{20}$ overlay

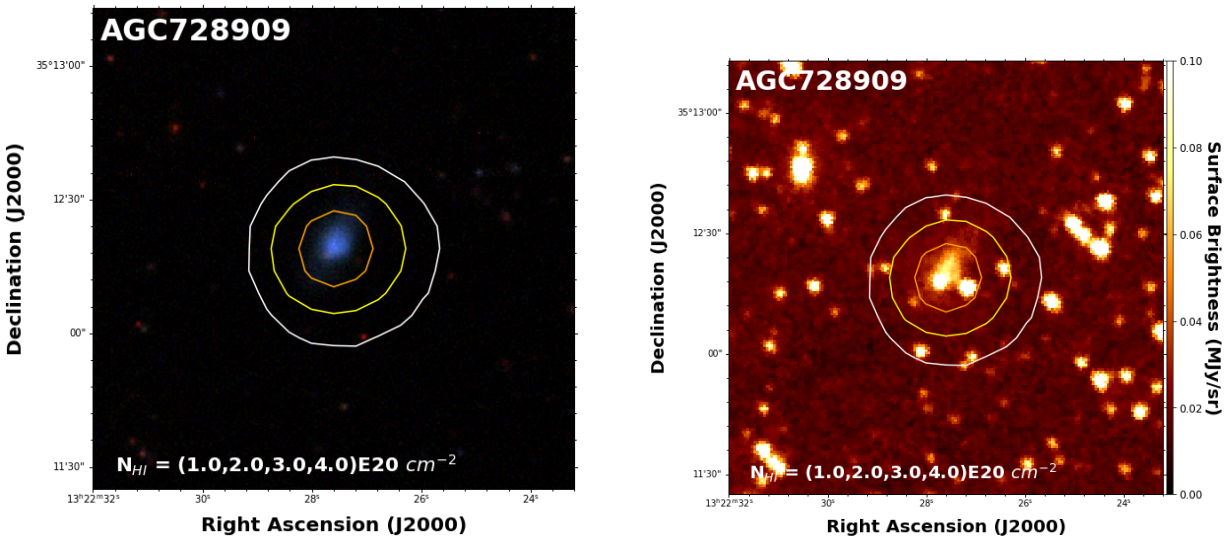

Figure 34. AGC 728909 (Left) three color Legacy Survey image with $1e^{20}$ contour overlay. (Right) Spitzer 3.6 µm image with moment $1e^{20}$ overlay

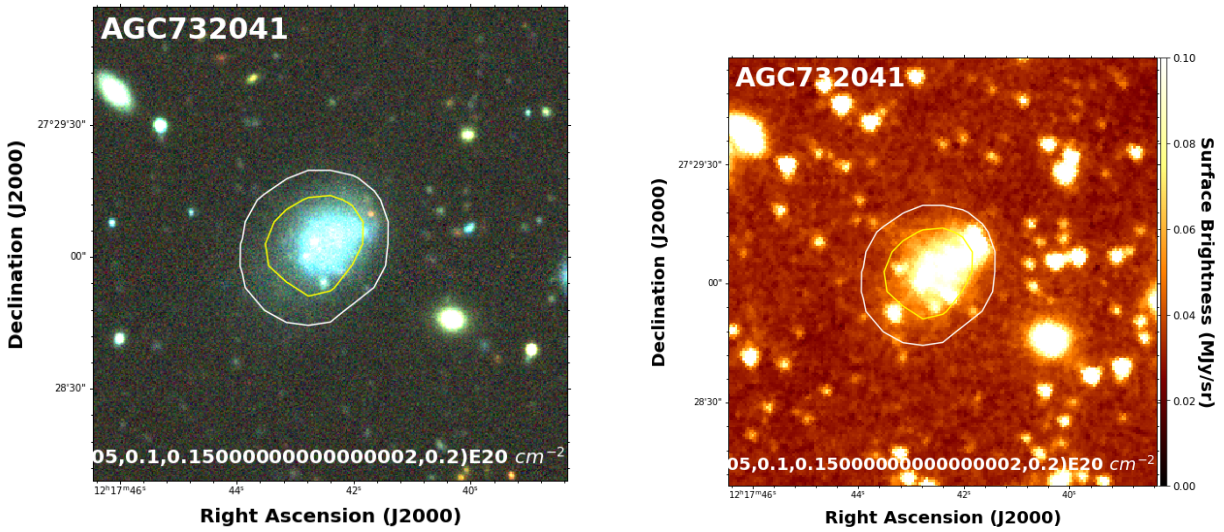

Figure 35. AGC 732041 (Left) three color Legacy Survey image with $1e^{20}$ contour overlay. (Right) Spitzer 3.6 µm image with moment $1e^{20}$ overlay

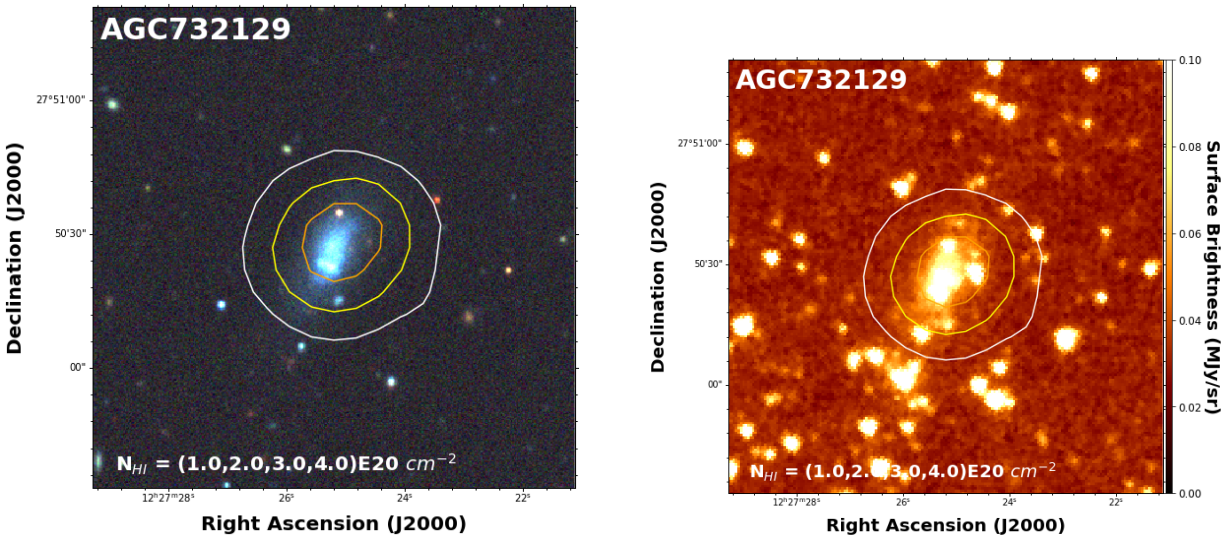

Figure 36. AGC 732129 (Left) three color Legacy Survey image with $1e^{20}$ contour overlay. (Right) Spitzer 3.6 µm image with moment $1e^{20}$ overlay

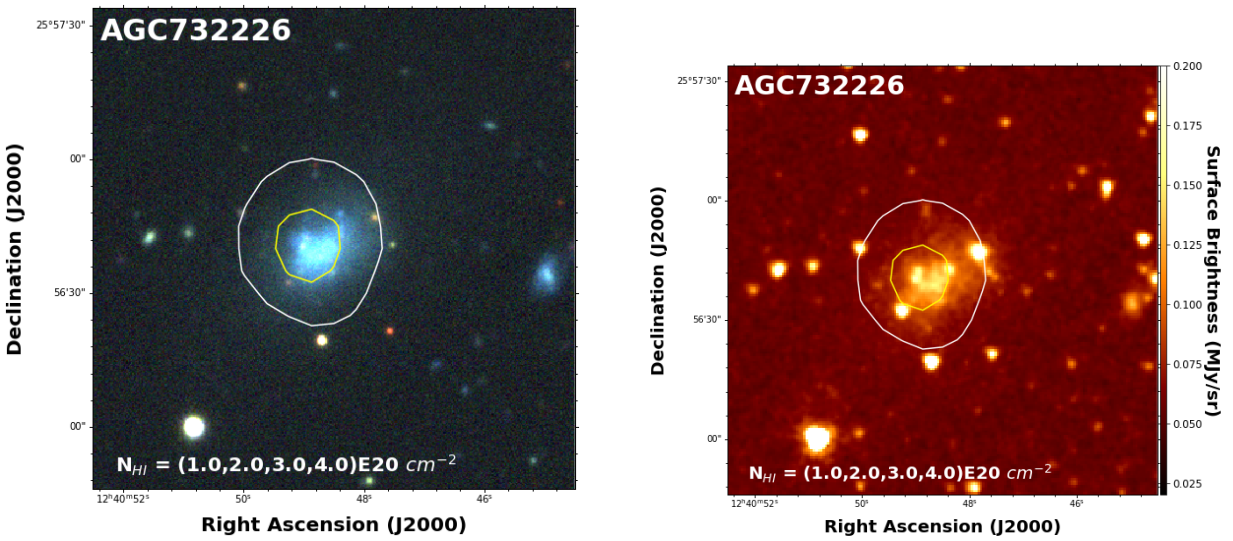

Figure 37. AGC 732226 (Left) three color Legacy Survey image with $1e^{20}$ contour overlay. (Right) Spitzer 3.6 µm image with moment $1e^{20}$ overlay

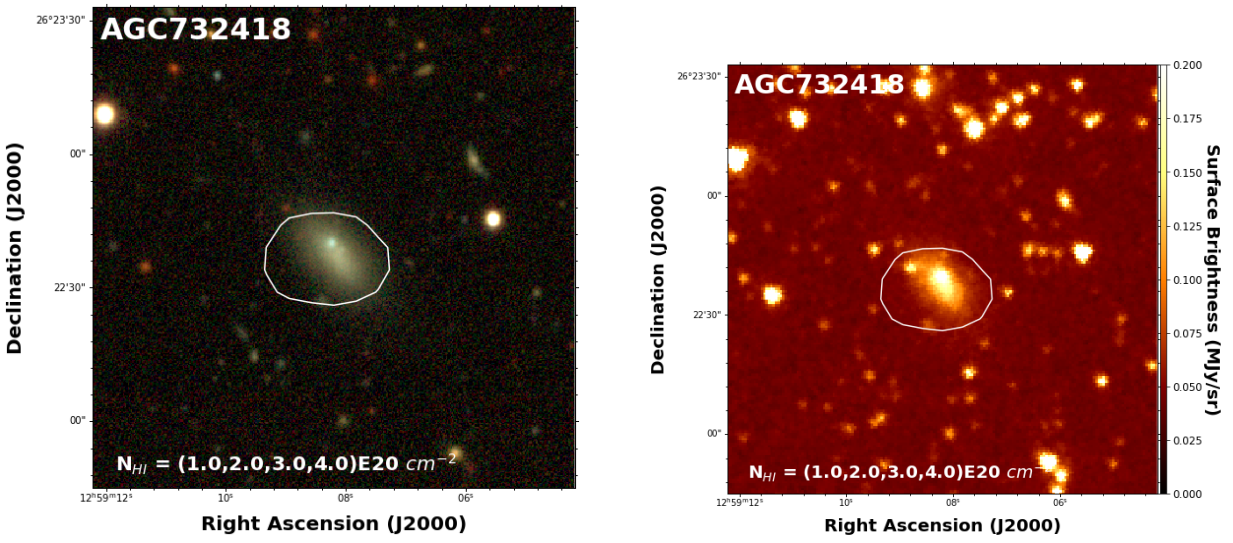

Figure 38. AGC 732418 (Left) three color Legacy Survey image with $1e^{20}$ contour overlay. (Right) Spitzer 3.6 µm image with moment $1e^{20}$ overlay